80-FM-6

JSC-16333

JAN 14 1980

Solar Maximum Mission Panel Jettison Analysis

Remote Manipulator System Interaction

Mission Planning and Analysis Division

January 1980

National Aeronautics and Space Administration

Lyndon B. Johnson Space Center
Houston, Texas

80-FM-6

JSC-16333

SHUTTLE PROGRAM

SOLAR MAXIMUM MISSION PANEL JETTISON ANALYSIS

REMOTE MANIPULATOR SYSTEM INTERACTION

By R. B. Bauer
McDonnell Douglas Technical Services Co., Inc.
JSC Task Monitor: C. Gott, Flight Analysis Branch

Approved: Morris V. Jenkins
Morris V. Jenkins, Chief
Flight Analysis Branch

Approved: Ronald L. Berry
Ronald L. Berry, Chief
Mission Planning and Analysis Division

Mission Planning and Analysis Division

National Aeronautics and Space Administration

Lyndon B. Johnson Space Center

Houston, Texas

January 1980

CONTENTS

LIST OF FIGURES

LIST OF FIGURES

LIST OF TABLES

LIST OF ACRONYMS AND SYMBOLS

A	Fulcrum hinge
$(\underline{b})$	Kickoff spring location vector
CM	Center of Mass
EE	End Effector
EP	Elbow Pitch
F	Spring force
F_1	Component of F in payload X direction
F_2	Component of F in payload Y direction
F_3	Component of F in payload Z direction
FOD	Flight Operations Directorate
$\overline{H}$	Orbiter angular momentun vector
HGAS	High Gain Antenna System
(I)	Panel inertia matrix with respect to $\underline{s}$
(I')	Panel inertia matrix with respect to $\underline{p}'$
k_{ls}	Kickoff spring linear rays
k_s	Kickoff spring rotational constant
LVLH	Local Vertical Local Horizontal
MDTSCO-HAD	McDonnell Douglas Technical Services Company Houston Astronautics Division
M_p	Jettisonable mass
MPM	Manipulator Position Mechanism
MPM/LON	Manipulator Position Mechanism/Longeron Interface
$\underline{p}$	Panel axes coordinate system unit vector
$\underline{p}'$	Hinge axes coordinate system unit vecotr
PDRS	Payload Deployment and Retrieval System
PDRSS	Payload Deployment and Retrieval Systems Simulation
PL	Payload

LIST OF ACRONYMS AND SYMBOLS (Continued)

POR	Point of Resolution
PYR	Pitch, yaw, roll
R	Reaction force
R_1	Component of R in payload X direction
R_2	Component of R in payload Y direction
R_3	Component of R in payload Z direction
$\bar{R}$	Orbiter/Earth radius vector
RI/SPAR	Rockwell International/Spar interface
$(\underline{r})$	Fulcrum hinge location vector
r_{1s}	Kickoff spring moment arm
RMS	Remote Manipulator System
$\underline{s}$	Spacecraft axes coordinate system unit vector
SMM/MMS	Solar Maximum Mission/Multi Mission Satellite
SP	Shoulder Pitch
SY	Shoulder Yaw
t	Time in seconds
T_A	Reaction torque at A
T_{A1}	Component of T_A in payload X direction
T_{A2}	Component of T_A in payload Y direction
T_{A3}	Component of T_A in payload Z direction
$\bar{V}$	Orbiter velocity vector
WP	Wrist Pitch
WR	Wrist Roll
WY	Wrist Yaw
w.r.t	with respect to
β	Panel natural frequency

LIST OF ACRONYMS AND SYMBOLS (Continued)

γ	Kickoff spring orientation relative to panel
ζ	Kickoff spring linear preload
θ	Panel rotation angle
θ_o	Initial panel rotation angle
θ_s	Panel rotation angle at separation
$\dot{\theta}$	Panel angular velocity
$\ddot{\theta}$	Panel angular acceleration
θ_F	Direction of F relative to payload coordinate system
θ_R	Direction of R relative to payload coordinate system
θ_{T_A}	Direction of T_A relative to payload coordinate system
ϕ	Panel droop angle
ψ	Panel tilt angle

1.0 SUMMARY

A study has been made to develop Remote Manipulator System (RMS) configurations for jettison of the solar panels on the Solar Maximum Mission/Multi Mission Satellite (SMM/MMS). A valid RMS maneuver between jettison configurations has also been developed. Arm and longeron loads and end effector excursions due to the solar panel jettison have been determined to see if they are within acceptable limits. These loads and end effector excursions have been analyzed under two RMS modes, servos active in position hold submode, and in the brakes on mode.

Significant conclusions and recommendations resulting from this study are as follows:

(1) The loads on the RMS resulting from the jettisoning of the solar panels are well within the limits of the RMS for the configurations analyzed in this study, even though one of those configurations is near a wrist yaw singularity.

(2) The motion of the payload due to solar panel jettison is negligible.

(3) There is no difference in loads and end effector excursions between otherwise similar configurations analyzed in the position hold mode or in the brakes on mode. This is because the loads about the joint drive axes never get larger than the motor static friction level and thus, the joints do not move.

The decisions to use the primary or alternate jettison configuration and to use the position hold mode or the brakes on mode should be based on considerations other than RMS structural loads due to solar panel jettison.

A brief description of the problem is made in Section 2.0. An outline of the steps necessary to and leading up to the analysis is laid out in Section 3.0. The necessary assumptions are made in Section 3.1. SMM/MMS mass properties are defined in Section 3.2. Mathematical models of the loads are given and curve fits are developed in Section 3.3. In Section 3.4 a primary and an alternate jettison configuration are discussed which satisfy Orbiter attitude, direction of jettison, SMM/Orbiter relative attitude and field of view constraints. Acceptable RMS arm configurations are found for both the primary and alternate jettison configurations for jettisoning both the +Y and -Y solar panels and RMS auto sequences are developed to go from the arm configuration for jettisoning the +Y panel to the arm configuration for jettisoning the -Y panel for both the primary and alternate configurations. Section 4.0 covers the Payload Deployment and Retrieval Systems Simulation (PDRSS) analysis of the jettison simulations. Peak loads and end effector excursions are determined. Conclusions and Recommendations are made in Section 5.0. References are listed in Section 6.0.

2.0 INTRODUCTION

The Solar Observatory of the first SMM/MMS is scheduled to be retrieved by a Shuttle Orbiter in 1982. The solar arrays of the observatory are not retractable and hence require jettisoning prior to stowing the observatory in the Orbiter's payload bay.

Once grappled, the payload must be properly oriented by the RMS for jettison of the first solar panel. It is desired to jettison both panels in a retrograde direction. Therefore, it is necessary to reorient the payload for jettison of the second panel. A valid RMS maneuver for this will be developed in this study.

During the jettison sequence, loads are exerted on the SMM/MMS and consequently on the RMS. At a meeting of the Payload Safety Review Panel on July 11, 1979, a question was brought up as to the severity of these loads and whether or not the RMS can withstand them. Also of concern are end effector excursions due to these loads. The loads and end effector excursions will be examined in this study to determine if they are tolerable.

Whether to jettison the panels with the RMS in the brakes on mode or with servos active in the positin hold submode is also a matter which will be examined in this study.

3.0 DISCUSSION

In order to assume that this study provides accurate information, certain basic assumptions must be made. The assumptions concerning SMM/MMS mass properties, RMS configurations, and supporting mathematical model development are presented in this section.

3.1 ASSUMPTIONS

It is assumed that the SMM/MMS can be grappled with both solar arrays in their operational configuration, and that once grappled, the SMM/MMS can be maneuvered by the RMS to either of the jettison configurations designated in this study. It is also assumed that once the SMM/MMS is grappled, the Orbiter can maneuver to either of the Orbiter attitudes designated in this study for solar panel jettison.

It is assumed that information provided in References 3 and 4 supersedes that provided in Reference 2 when applicable.

The jettisonable mass has been increased from that noted in Reference 2.0. For purposes of computing the new panel inertia matrix (I) in Section 3.3, it is assumed that the mass increase is uniform throughout the panel.

It is assumed that the jettisonable mass of each of the solar arrays is equal and that the magnitude of the loads due to solar panel jettison are the same for each panel.

The SMM/MMS has a High Gain Antenna System (HGAS) which is to be retracted into the SMM/MMS before grappling. In the event of a malfunction and the HGAS cannot be retracted, it will be jettisoned. Due to the small weight of the HGAS relative to the SMM/MMS, it is assumed that the lack of the HGAS will not change the mass properties of the SMM/MMS enough to significantly affect the results.

For the PDRSS analysis, a massless, flexible RMS is assumed. One of the configurations analyzed is near a singularity in the wrist yaw joint. In this case, the PDRSS flexibility model becomes unstable. In order to execute a successful PDRSS analysis for this case, it was necessary to assume a rigid boom model of the RMS. However, the gearbox flexibility was still included.

The RMS response to the solar panel jettisons was analyzed assuming servos active in the position hold submode and then analyzed again assuming the brakes on mode.

3.2 SMM/MMS MASS PROPERTIES AND COORDINATE SYSTEMS

The SMM/MMS mass properties listed in Tables I-III are taken from Reference 3.

The payload coordinate system used in this study (Fig. 1) has its YZ plane at the level of the grapple fixture. The X axis is along the centerline

of the payload. The origin of this coordinate system is 2.73 ft. from the end effector. The payload CG is not at the origin or along the centerline of the payload.

Figure 2 shows the hinge axes system $\underline{p}'$ compared to the spacecraft axes system $\underline{s}$. Figure 3 shows the solar array system operational position with the solar panel in the panel axes system $\underline{p}$. $\underline{s}$, $\underline{p}$, and $\underline{p}'$, are unit vectors. Note that in the $\underline{p}'$ system the panel is only rotated whereas in the $\underline{p}$ system the panel is rotated, drooped, and tilted. During the panel jettison, the rotation angle θ changes, but the droop ϕ, and the tilt Ψ remain constant.

TABLE I

SMM + MMS MASS PROPERTIES

(Orbital Configuration with HGAS Stowed)

Total Mass = 2247.8 kg ≡ 4955.6 lbs.

CM Relative to Payload Coordinate System

$\bar{x}$ = 1.2683 m = 4.16 ft = 49.93 in

$\bar{y}$ = -.0013 m = -0.004 ft = -.05 in

$\bar{z}$ = .0202 m = .07 ft = .79 in

Total Inertia about CM

Ixx = 1838.0	Ixy = -97.5	Ixz = -185.3	
Iyx = -97.5	Iyy = 3610.2	Iyz = -134.7	(kg m^2)
Izx = -185.3	Izy = -134.7	Izz = 3786.3	
Ixx = 1355.6	Ixy -71.9	Ixz = -136.7	
Iyx = -71.3	Iyy = 2662.7	Iyz = -99.3	(slug ft^2)
Izx = -136.7	Izy = -99.3	Izz = 2792.6	

TABLE II

SMM + MMS MASS PROPERTIES

(HGAS Stowed, +Y Solar Array Jettisoned)

Total Mass = 2198.8 kg ≡ 4847.65 lbs.

CM Relative to Payload Coordinate System

$\bar{x}$	=	1.2725	m	=	4.17	ft	= 50.10 in.
$\bar{y}$	=	-.0491	m	=	-.16	ft	= -1.93 in.
$\bar{z}$	=	.0087	m	=	.03	ft	= .34 in.

Total Inertia about CM

Ixx = 1546.0		Ixy = -117.6		Ixz = -190.2		
Iyx = -117.6		Iyy = 3561.3		Iyz = 79.3		(kg m^2)
Izx = -190.2		Izy = 79.3		Izz = 3541.3		
Ixx = 1140.3		Ixy = -86.7		Ixz = -140.3		
Iyx = -86.7		Iyy = 2626.7		Iyz = -58.5		(slug ft^2)
Izx = -140.3		Izy = -58.5		Izz = 2611.9		

TABLE III

SMM + MMS MASS PROPERTIES

(Re-entry Configuration, HGAS Stowed, Solar Arrays Jettisoned)

Total Mass = 2149.9 kg ≡ 4739.7 lbs.

CM Relative to Payload Coordinate System

$\bar{x}$	= 1.2768 m	=	4.19 ft	=	50.27 in.
$\bar{y}$	= -.0014 m	=	-.01 ft	=	-.06 in.
$\bar{z}$	= .0211 m	=	.07 ft	=	.83 in.

Total Inertia about CM

Ixx = 1263.1		Ixy = -97.5		Ixz = -184.9		
Iyx = -97.5		Iyy = 3510.9		Iyz = -22.1		(kg m^2)
Izx = -184.9		Izy = -22.1		Izz = 3306.9		
Ixx = 931.6		Ixy = -71.9		Ixz = -126.4		
Iyx = -71.9		Iyy = 2589.5		Iyz = -16.3		(slug ft^2)
Izx = -136.4		Izy = -16.3		Izz = 2439.0		

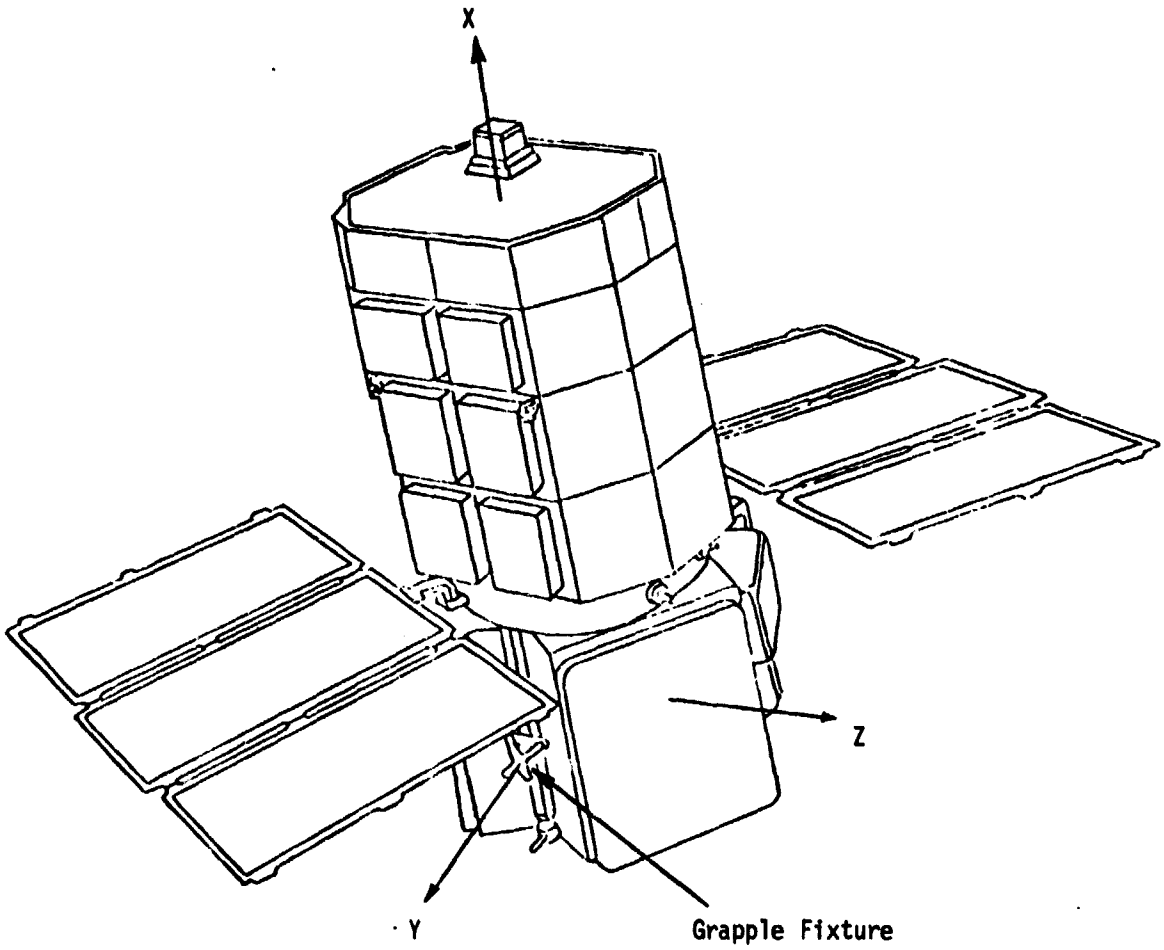

YZ Plane is at level at grapple fixture

+Y Coming out of grapple fixture

+X Coming out of top at satellite

Fig. 1

SMM/MMS COORDINATE SYSTEM

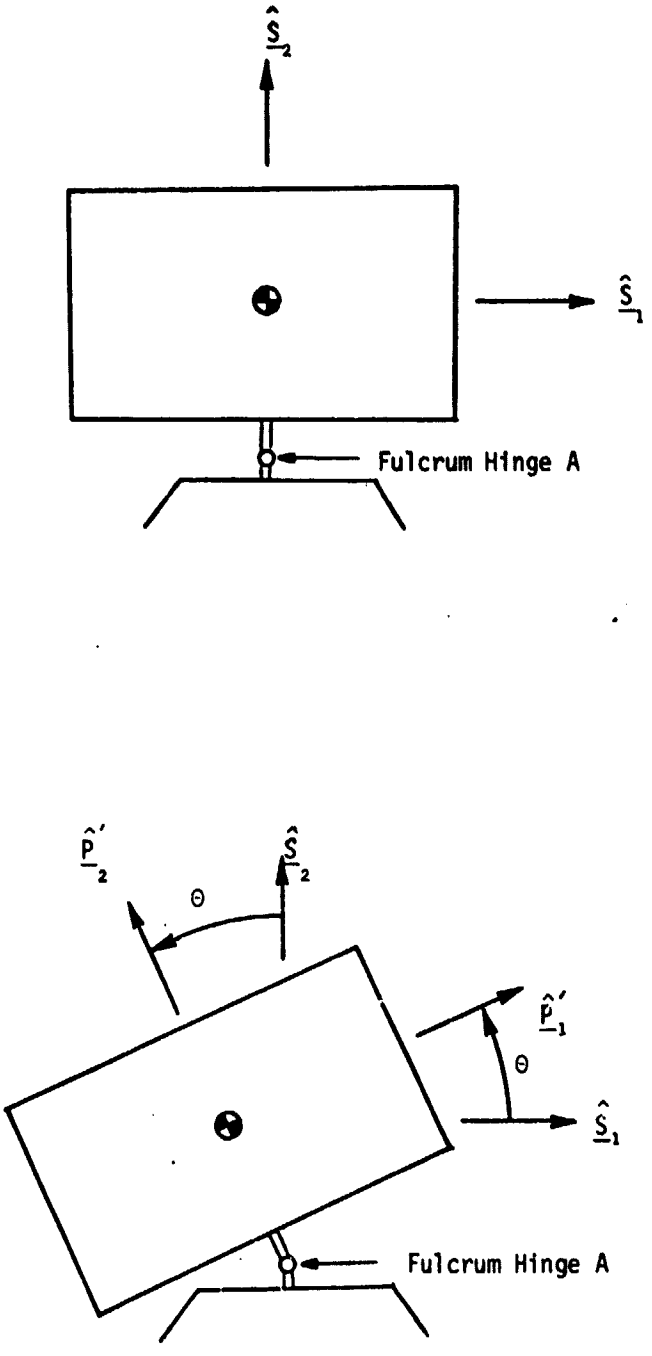

Fig. 2
Spacecraft Axes System $\hat{S}$ and
Hinge Axes System $\hat{P}'$

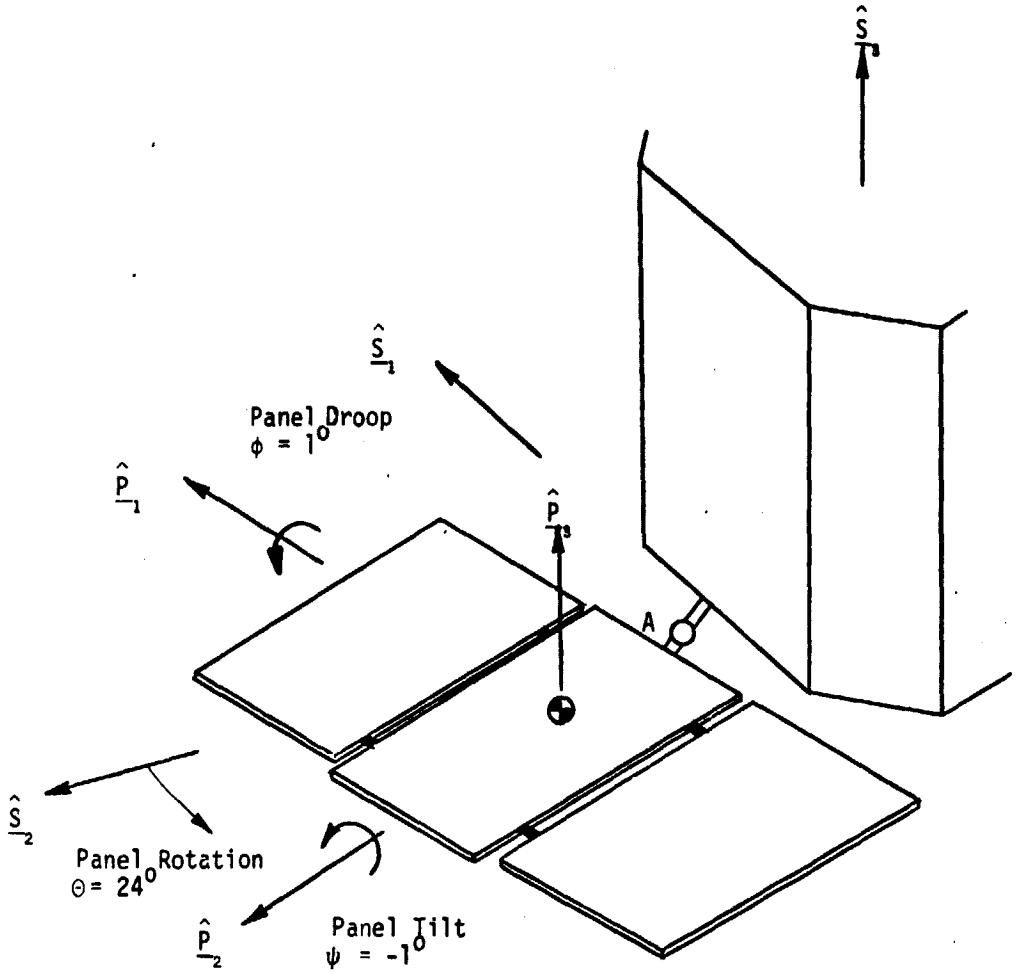

Fig. 3

SOLAR ARRAY SYSTEM OPERATIONAL POSITION
SPACECRAFT AXES SYSTEM $\hat{S}$
PANEL AXES SYSTEM $\hat{P}$

3.3 CALCULATION OF TIME HISTORY OF SPRING FORCE, REACTION FORCE, AND REACTION TORQUE ON SMM/MMS BY SOLAR PANEL JETTISON

The jettison sequence was simulated by modeling the solar array system as a single rigid body, initially attached to an inertially fixed spacecraft. At t=0, release of the kickoff spring preload is initiated, and the panel begins a clockwise rotation about the fulcrum hinge, which is assumed to be frictionless. When the spring has extended to its equilibrium position, the panel is separated. Thereafter, it continues in a trajectory determined by the instantaneous translational and rotational rates at separation. Figure 4 depicts the jettison sequence with the accompanying loads on the SMM/MMS. Note that the panel is slung away from the satellite like a frisbee rather than being pushed straight out. Figure 5 shows the jettison mechanism. Figure 6 shows a panel free body diagram.

The weight of the SMM/MMS in orbital configuration with HGAS stowed is 4955.6 lbs. The weight of the SMM/MMS in re-entry configuration with HGAS stowed and both solar panels jettisoned is 4739.7 lbs. From this we can compute the jettisonable mass (Mp) of each solar array to be 3.355 slugs.

Reference 2 gives a jettisonable mass of 2.64 slugs. It also gives a solar panel inertia matrix (I). But these figures are no longer accurate. By multiplying the panel inertia matrix by the ratio of the new jettisonable mass over the old jettisonable mass, a reasonably accurate panel inertia matrix can be obtained.

(I) is the panel inertia matrix fixed in the spacecraft or $\underline{s}$ reference frame. (I') is the panel inertia matrix fixed in the hinge or $\underline{p}'$ reference frame (See Fig. 2). (I') can be computed from (I) as follows:

$$(I') = [(C(\phi))\ (C(\Psi))]\ (I)[(C(\phi))\ (C(\Psi))]^T$$

where

$$(C(\phi)) = \begin{bmatrix} 1 & 0 & 0 \\ 0 & \cos\phi & -\sin\phi \\ 0 & \sin\phi & \cos\phi \end{bmatrix}$$

and

$$(C(\Psi)) = \begin{bmatrix} \cos\Psi & 0 & \sin\Psi \\ 0 & 1 & 0 \\ -\sin\Psi & 0 & \cos\Psi \end{bmatrix}$$

$\phi = -1^o$ (panel droop) and $\Psi = 1^o$ (panel twist) remain constant throughout the panel rotation through θ.

The only elements of (I') necessary for this study are I'_{13}, I'_{23}, and I'_{33}. These are used in the calculations of β, panel natural frequency, R, reaction force, and T_A, reaction torque.

Table IV tabulates the pertinent solar array system jettison data. With certain corrections, this data comes from the Hughes document (Ref. 2).

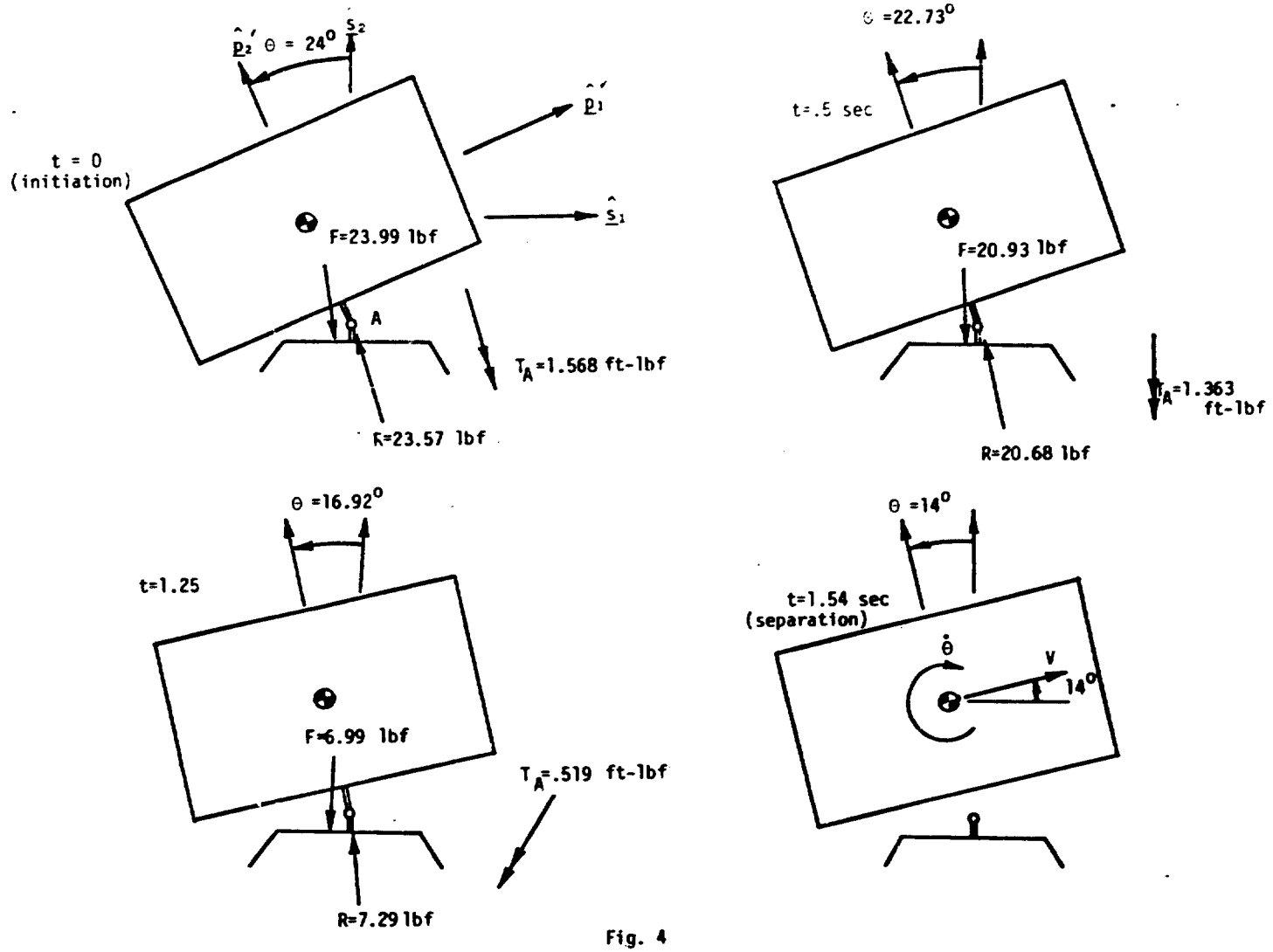

Fig. 4

SMM/MMS PANEL JETTISON SEQUENCE WITH ACCOMPANYING LOADS ON SMM/MMS

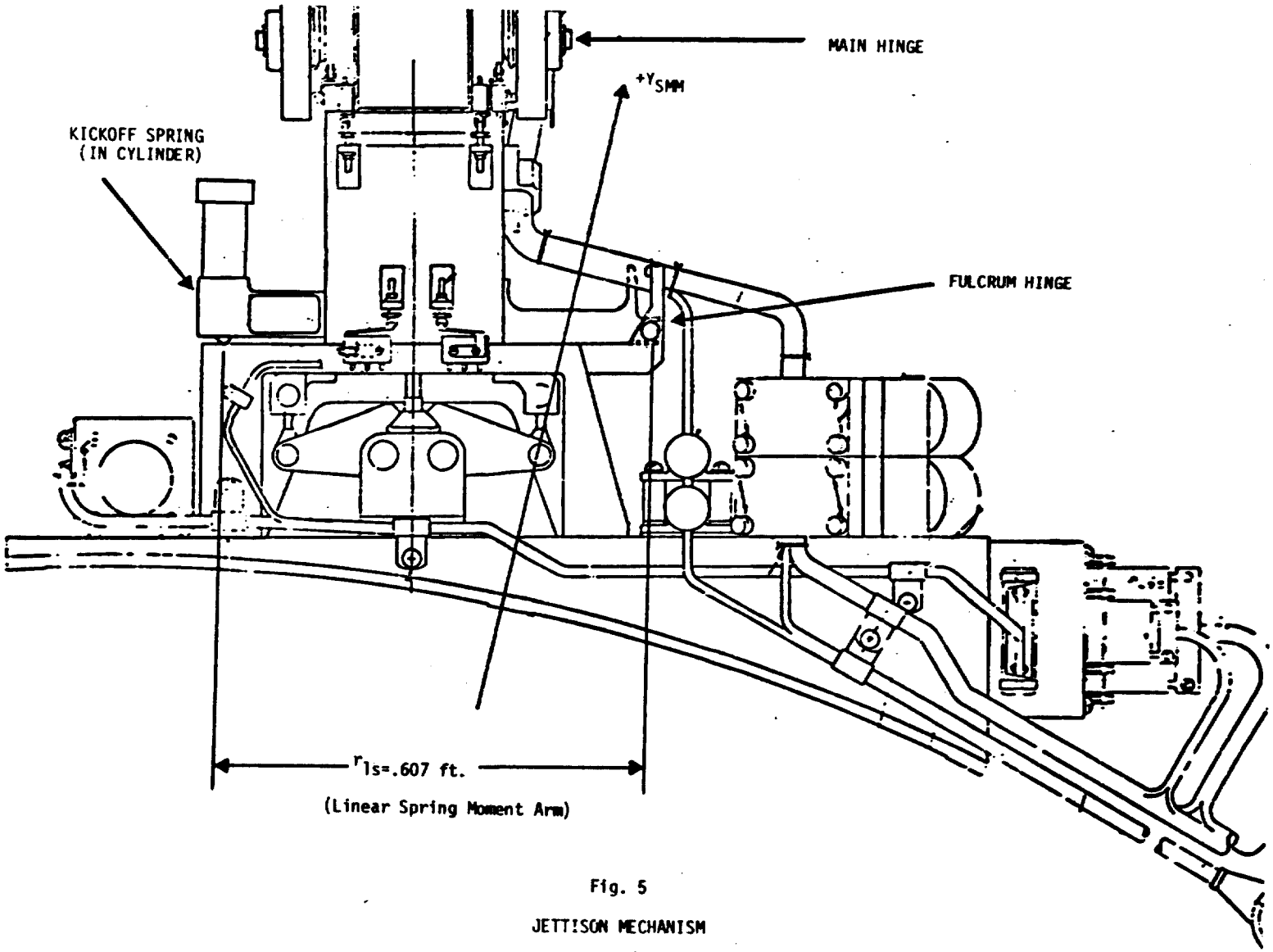

Fig. 5

JETTISON MECHANISM

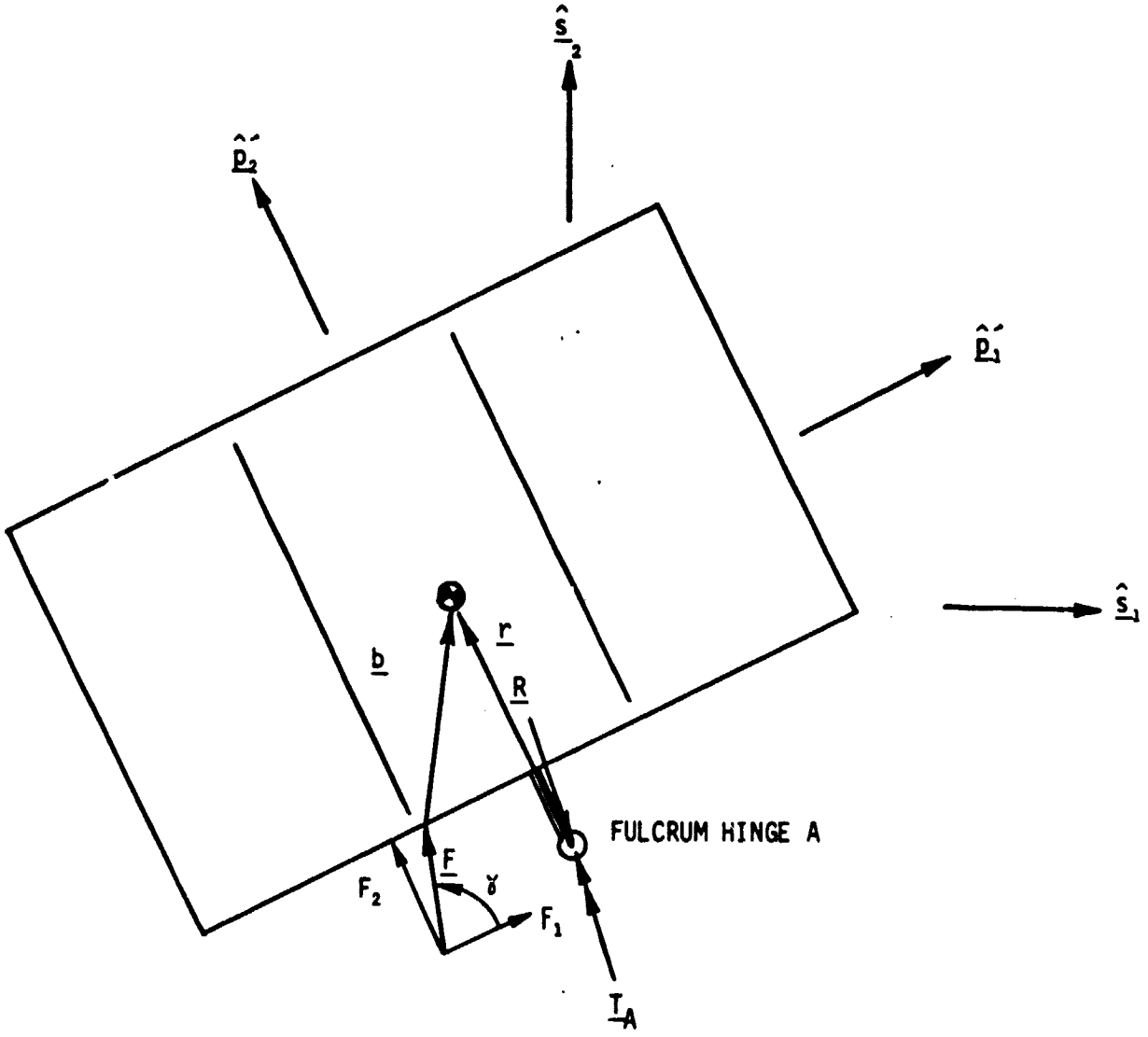

Fig. 6

PANEL FREE BODY DIAGRAM

TABLE IV

SOLAR ARRAY SYSTEM JETTISON DATA

Panel Mass (Jettisonable)		m_s = 3.355 slugs
Panel Orientation (Initial Rotation)		θ_o = 24°
	(Separation)	θ_s = 14°
	(Droop)	ϕ = -1°
	(Tilt)	Ψ = 1°
Kickoff Spring	(Linear Rate)	k_{ls} = 226.4 lbf/ft
	(Linear Preload)	ζ = .106 ft
	(Moment Arm)	r_{ls} = .607 ft
	(Rotational Constant)	k_s = 137.425 lbf
	(Orientation)	γ = 78°
	(Location)	$(\underline{b})$ = (.667 3.271 .585) ft
	(w.r.t $\underline{p}'$)	
Fulcrum Hinge (Location) (w.r.t. $\underline{p}'$)		$(\underline{r})$ = (0.0 4.417 .585) ft
Panel Natural Frequency		β = 1.02 1/sec
Panel Inertia Matrix	$(I) = \begin{bmatrix} 14.06 & 0 & 0 \\ 0 & 36.74 & -.20 \\ 0 & -.20 & 52.66 \end{bmatrix}$	sl-ft^2
Panel Inertia (w.r.t. $\underline{p}'$)	I'_{13} = .67 (sl-ft^2)	
	I'_{23} = .08 (sl-ft^2)	
	I'_{33} = 52.65 (sl-ft^2)	

After the panel rotates through 10° the jettison spring is in its equilibrium position and panel separation occurs at t = 1.54 sec.

The equations for θ, $\dot{\theta}$, $\ddot{\theta}$, the spring force, F, the reaction force, R, and the reaction torque, T_A, are given as functions of time in Table V. These equations were derived in the Hughes document (Ref. 2). Figures 7a, 7b, and 7c show the direction of application of F, R, and T on the SMM/MMS. The results of the equation in Table V are tabulated in Table VI. F, R, and T are resolved into orthogonal components parallel to the payload coordinate system. These components are tabulated in Table VII.

Using the 3rd order method of least squares curve fit, the orthogonal components of F, R, and T_A tabulated in Table VII are developed into equations representing the magnitude of these components as functions of time. These equatons are given in Table VIII. The curves from these equations for F(t), R(t), and $T_A(t)$ are plotted in Figures 8, 9, and 10 respectively. As can be seen, the curves fit reasonably close to the original data points from which the curve fits were generated. These data points are represented by circles on the plots.

These equations will be used in PDRSS to simulate the loads exerted by the jettisoning panels on the SMM/MMS.

TABLE V

EQUATIONS

(F, R, and T_A are acting on Panel in $\underline{p}'$ Reference Frame)

$$\theta(t) = (\theta_o - \theta_s) \cos \beta t + \theta_s \quad \text{(deg)}$$

$$\dot{\theta}(t) = -\frac{\pi}{180} (\theta_o - \theta_s) \beta \sin \beta t \quad \frac{\text{(rad)}}{\text{sec}}$$

$$\ddot{\theta}(t) = -\frac{\pi}{180} (\theta_o - \theta_s) \beta^2 \cos \beta t \quad \frac{\text{(rad)}}{\text{sec}^2}$$

$$F_1(t) = K_s \frac{\pi}{180} (\theta(t) - \theta_s) \cos \gamma \quad \text{(lbf)}$$

$$F_2(t) = K_s \frac{\pi}{180} (\theta(t) - \theta_s) \sin \gamma \quad \text{(lbf)}$$

$$F_3(t) = 0 \quad \text{(lbf)}$$

$$R_1(t) = -M_p (r_2 \ddot{\theta}(t) + r_1 \dot{\theta}^2(t)) - F_1(t) \quad \text{(lbf)}$$

$$R_2(t) = M_p (r_1 \ddot{\theta}(t) - r_2 \dot{\theta}^2(t)) - F_2(t) \quad \text{(lbf)}$$

$$R_3(t) = 0 \quad \text{(lbf)}$$

$$T_{A1}(t) = I'_{13} \ddot{\theta}(t) - I'_{23} \dot{\theta}^2(t) - b_3 F_2(t) + b_2 F_3(t) - r_3 R_2(t) + r_2 R_3(t) \quad \text{(ft lbf)}$$

$$T_{A2}(t) = I'_{23} \ddot{\theta}(t) + I'_{13} \dot{\theta}^2(t) + b_3 F_1(t) - b_1 F_3(t) + r_3 R_1(t) - r_1 R_3(t) \quad \text{(ft lbf)}$$

$$T_{A3}(t) = 0 \quad \text{(ft lbf)}$$

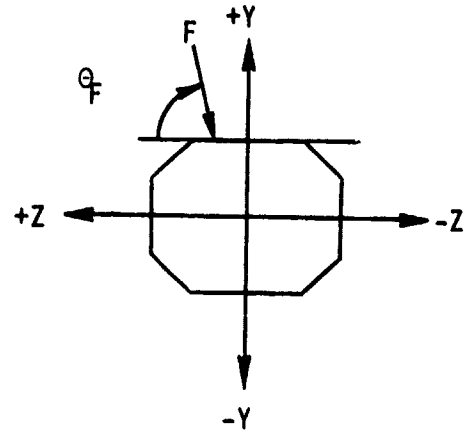

Fig. 7a

F, Θ_F

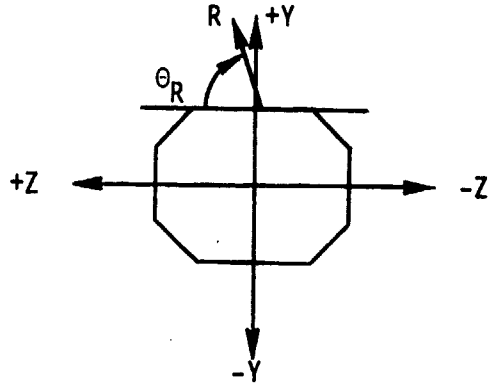

Fig. 7b

R, Θ_R

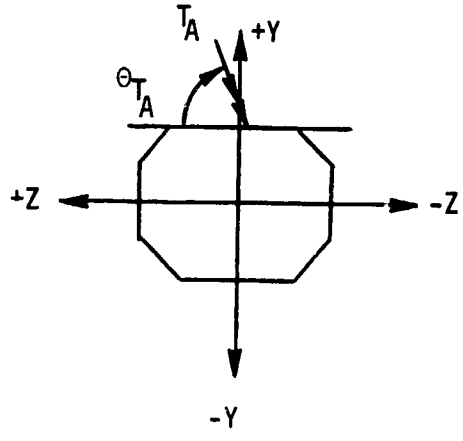

Fig. 7c

T_A , Θ_{T_A}

Figs. 7a, 7b, 7c

TABLE VI

Data from Jettison of +Y Panel

(F, R, and T_A are acting on SMM/MMS in $\underline{p}'$ Reference Frame)

t(sec)	θ(deg)	$\dot{\theta}$ $\frac{rad}{sec}$	$\ddot{\theta}$ $\frac{rad}{sec^2}$	F_1(lbf)	F_2(lbf)	F(lbf)	θ_F(deg)
0.00	24.00	0.00	-.18	-4.99	-23.46	23.99	78.00
0.25	23.68	-.04	-.18	-4.83	-22.70	23.21	78.32
0.50	22.73	-.09	-.16	-4.35	-20.48	20.93	79.27
0.75	21.21	-.12	-.13	-3.60	-16.92	17.30	80.79
1.00	19.23	-.15	-.10	-2.61	-12.28	12.55	82.77
1.25	16.92	-.17	-.05	-1.45	- 6.84	6.99	85.08
1.50	14.41	-.18	-.01	-0.20	- 0.96	0.98	87.59
1.54	14.00	-.18	0.00	0.00	0.00	0.00	

t(sec)	θ(dg)	$\dot{\theta}$ $\frac{rad}{sec}$	$\ddot{\theta}$ $\frac{rad}{sec^2}$	R_1(lbf)	R_2(lbf)	R(lbf)	θ_R(deg)
0.00	24.00	0.00	-.18	2.29	23.46	23.57	84.43
0.25	23.68	-.04	-.18	2.22	22.73	22.84	84.43
0.50	22.73	-.09	-.16	2.01	20.59	20.68	84.42
0.75	21.21	-.12	-.13	1.66	17.15	17.23	84.48
1.00	19.23	-.15	-.10	1.20	12.62	12.68	84.56
1.25	16.92	-.17	-.05	.67	7.26	7.29	84.74
1.50	14.41	-.18	-.01	.10	1.42	1.43	86.02
1.54	14.00	-.18	0.00	0.00	0.00	0.00	

t(sec)	θ(deg)	$\dot{\theta}$ $\frac{rad}{sec}$	$\ddot{\theta}$ $\frac{rad}{sec}$	T_{A1}(ftlbf)	T_{A2}(ftlbf)	T_A(ftlbf)	θT_A(deg)
0.00	24.00	0.00	-.18	+.123	-1.564	1.568	61.52
0.25	23.68	-.04	-.18	+.101	-1.513	1.517	62.50
0.50	22.73	-.09	-.16	+.042	-1.362	1.363	65.50
0.75	21.21	-.12	-.13	-.040	-1.135	1.136	70.83
1.00	19.23	-.15	-.10	-.133	- .832	.842	79.82
1.25	16.92	-.17	-.05	-.210	- .475	.519	96.96
1.50	14.41	-.18	-.01	-.265	- .082	.277	148.46
1.54	14.00	-.18	0.00	0.00	0.00	0.00	

TABLE VII

Components of Spring Force F, Reaction Force R, and Reaction Torque T_A on SMM/MMS by Jettison of +Y Panel in $\underline{s}$ Reference Frame

t(sec)	F(lbf)	Θ_F(deg)	F_Z(lbf)	F_Y(lbf)
0.00	23.99	78.00	-4.99	-23.46
0.25	23.21	78.32	-4.70	-22.73
0.50	20.93	79.27	-3.90	-20.57
0.75	17.30	80.79	-2.77	-17.08
1.00	12.55	82.77	-1.58	-12.45
1.25	6.99	85.08	- .60	- 6.97
1.50	0.98	87.59	- .04	- .98
1.54	0.00		0.00	0.00

t(sec)	R(lbf)	Θ_R(deg)	R_Z(lbf)	R_Y(lbf)
0.00	23.57	84.43	2.29	23.46
0.25	22.84	84.43	2.22	22.73
0.50	20.68	84.42	2.01	20.59
0.75	17.23	84.48	1.66	17.15
1.00	12.68	84.56	1.20	12.62
1.25	7.29	84.74	0.67	7.26
1.50	1.43	86.02	0.10	1.42
1.54	0.00		0.00	0.00

t(sec)	T_A(ftlbf)	ΘT_A(deg)	T_{A_Z}(ftlbf)	T_{A_Y}(ftlbf)
0.00	1.568	61.52	-.748	-1.379
0.25	1.517	62.50	-.700	-1.345
0.50	1.363	65.50	-.565	-1.240
0.75	1.136	70.83	-.373	-1.073
1.00	0.842	79.82	-.149	- .829
1.25	0.519	96.96	+.063	- .515
1.50	0.277	148.46	+.236	- .145
1.54	0.000		0.000	0.000

TABLE VIII

Equations for Spring Force F, Reaction Force R, and Reaction Torque T_A Acting on SMM/MMS During Jettison of +Y Panel. (Referenced to the Payload Coordinate System)

$$F(t)_Z = -4.98 - .34t + 6.35t^2 - 2.62t^3$$
$$F(t)_Y = -23.44 - .74t + 14.25t^2 - 2.52t^3$$

$$R(t)_Z = 2.28 + .13t - 1.52t^2 + .31t^3$$
$$R(t)_Y = 23.46 + .21t - 12.99t^2 + 1.98t^3$$

$$T_A(t)_Z = -.736 - .289t + 1.555t^2 - .656t^3$$
$$T_A(t)_Y = -1.381 + .058t + .408t^2 + .080t^3$$

$$t: 0 \rightarrow 1.54 \text{ sec}$$

The equations of F, R, and T_A for jettison of the -Y panel are the same as shown, but opposite in sign.

Points of Application (X, Y, Z) of F, R, and T_A on SMM/MMS (Referenced to the Payload Coordinate System)

+Y Panel Jettison	- Y Panel Jettison
F (3.06, 2.89, .47) ft.	F (3.06, -2.89, -.47) ft.
R (3.02, 3.03, -.12) ft.	R (3.02, -3.03, .12) ft.
T_A (3.02, 3.03, -.12) ft.	T_A (3.02, -3.03, .12) ft.

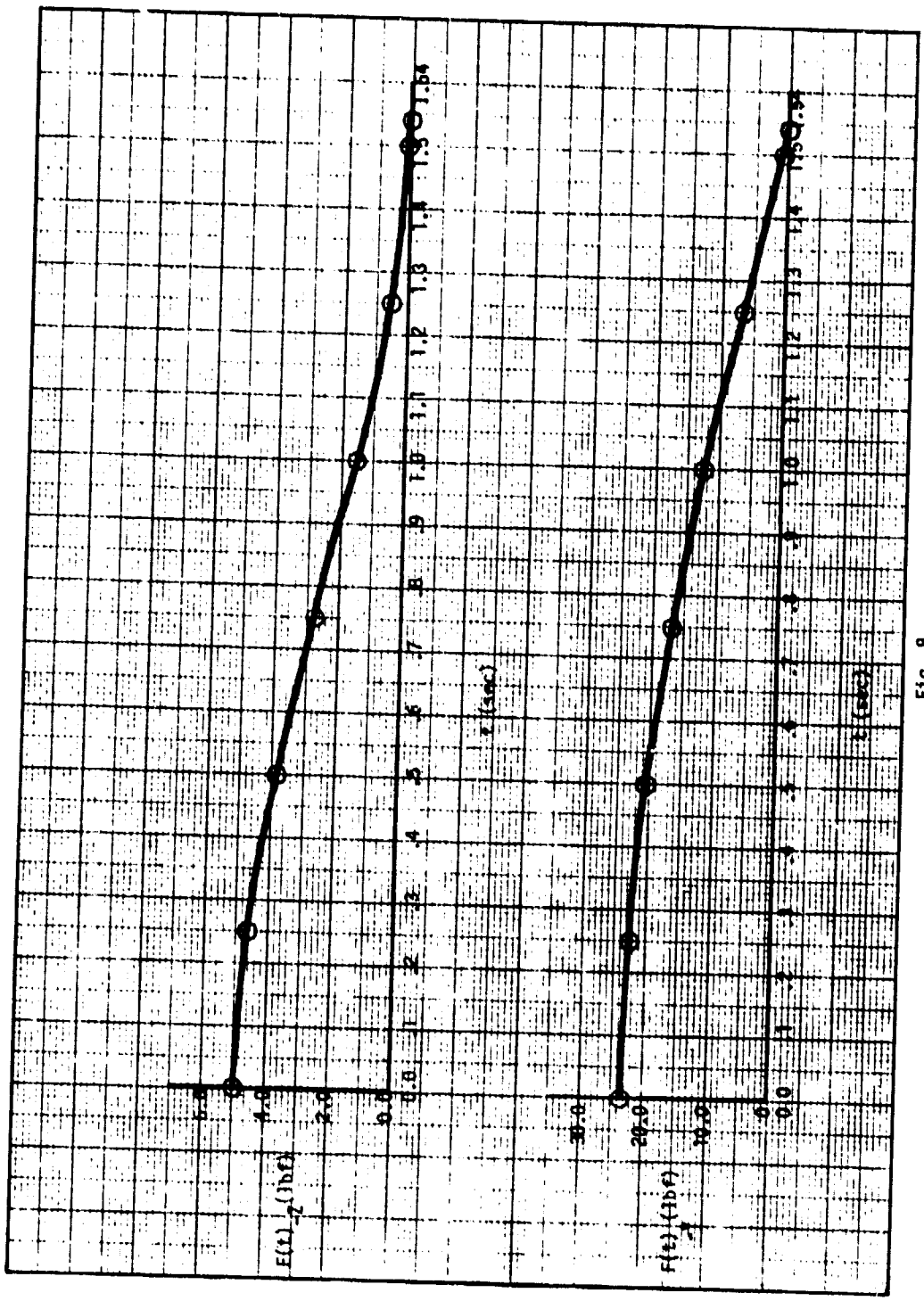

Fig. 8
SPRING FORCE VS. TIME
(PAYLOAD COORDINATE SYSTEM)

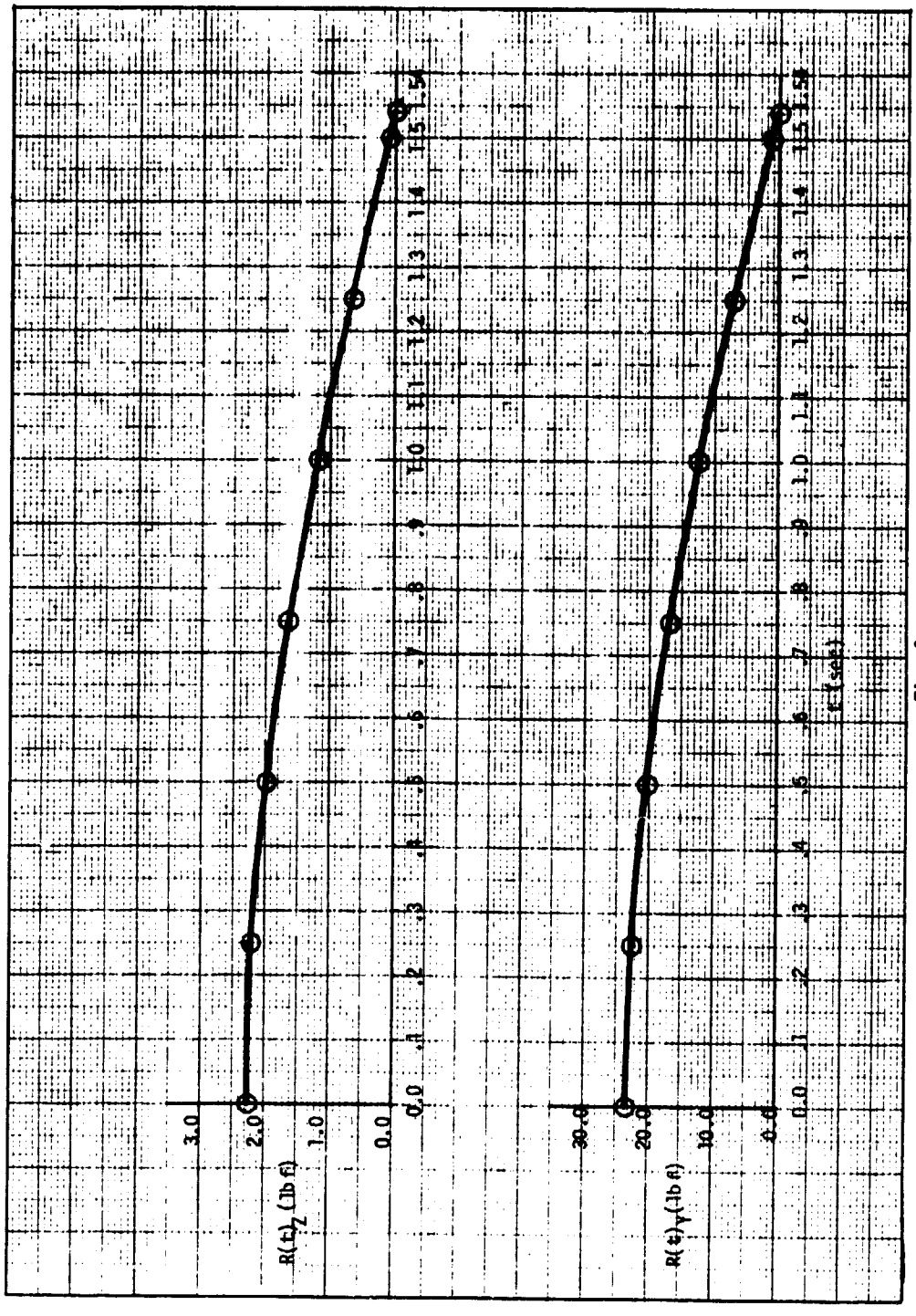

Fig. 9
REACTION FORCE VS. TIME
(PAYLOAD COORDINATE SYSTEM)

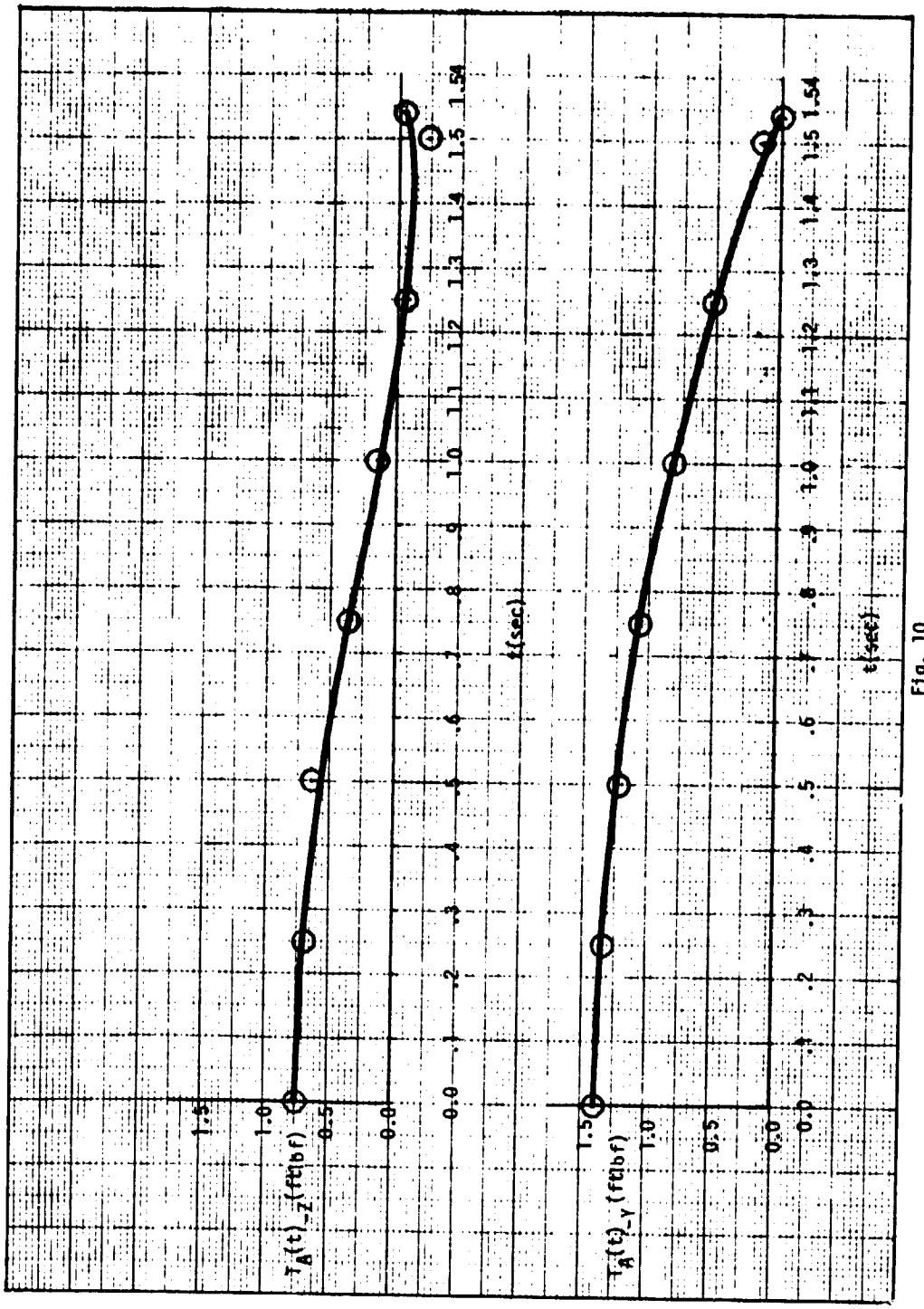

Fig. 10
REACTION TORQUE VS. TIME
(PAYLOAD COORDINATE SYSTEM)

3.4 JETTISON CONFIGURATIONS

In the recontact analysis study (Ref. 1), it was determined that the best direction of jettison is retrograde. This reduces the possibility of panel recontact with the Orbiter to a minimum.

A primary and an alternate jettison configuration were chosen by the Flight Operations Directorate (FOD) at the Johnson Space Center (Ref. 5). For each configurations there is a unique orbiter attitude (Fig. 11), and SMM/MMS attitude with respect to the Orbiter (Figs. 12 & 13). The panels are to be jettisoned one at a time with the +Y panel to be jettisoned first (Fig. 14). Then the payload is to be reoriented by means of an RMS maneuver so that the -Y panel can be jettisoned in the same direction as the +Y panel. Jettisoning the +Y panel, which is located directly above the grapple fixture, first, prevents problems with the +Y panel contacting the RMS during the RMS maneuver.

As pointed out in Reference 5, there is a possibility of the -Y panel being jettisoned when it was intended to jettison the +Y panel. This would send the -Y panel in the opposite direction that the +Y panel would have gone. Therefore, the jettison configurations were carefully chosen so that the panel will not contact the Orbiter in the event of an incorrect panel jettison. The possibility of recontact is increased with a posigrade jettison. The motion of a jettisoned panel relative to the Orbiter for posigrade jettisons is covered in Reference 1.

3.4.1 PRIMARY JETTISON CONFIGURATION

For the primary jettison configuration, the Orbiter is rotated through a 270^{o} yaw from the Local Vertical Local Horizontal (LVLH) system (Fig. 11). The payload is positioned above and slightly forward of the overhead observation windows. The +Y panel is jettisoned first. As can be seen in Figure 14, the panels jettison in opposite directions and at a 14^{o} offset from the payload Z coordinate axis. Therefore, it is necessary to reorient the payload for jettison of the -Y panel. This can be done either in the Manual Augmented Mode or as an auto sequence.

For this study, the payload reorientation was accomplished in a three stage RMS maneuver. The Point of Resolution (POR) is the origin of the payload coordinate system. It remains the same throughout the maneuver. Only the payload orientation is changed. Essentially, what the maneuver accomplishes is a 180^{o} roll and a 28^{o} yaw of the payload. In the final orientation the -Y panel is jettisoned and the payload is ready for berthing.

The position of the POR and the orientation of the payload for each stage of the RMS maneuver sequence are tabulated in Table IX in the coordinates to be used by the RMS fight software for an auto sequence. The POR is referenced to the Orbiter Body Axis System (Fig. 15) and the payload attitudes are referenced to the Orbiter Rotation Axis System (Fig. 15).

The joint angles and end effector positions and attitudes for the initial, final, and fly-by points for this maneuver are tabulated in Table X. Note that the coordinate system referenced to in this table is different

from that referenced to in Table IX.

Figures 16a through 16f, 17a through 17f, and 18a through 18f give a front, side, and top view respectively of the pictorial history of the primary configuration panel jettison sequence. The dotted lines are the overhead observation window fields of view.

3.4.2 ALTERNATE JETTISON CONFIGURATION

For the alternate jettison configuration, the Orbiter is rotated through a 90^{o} pitch and a 90^{o} roll from the LVLH system (Fig. 11). The payload is positioned above the cargo bay. The +Y panel is jettisoned first. The payload is then reoriented for jettison of the -Y panel. As before, this can be done either in the Manual Augmented Mode or as an auto sequence.

Again, the payload reorientation was accomplished in a three stage RMS maneuver. The POR is the origin of the payload coordinate system and remains the same throughout the maneuver. Only the payload orientation is changed. Essentially, what the maneuver accomplishes is a 180^{o} roll and a 28^{o} pitch of the payload. In the final orientation the -Y panel is jettisoned and the payload is ready for berthing.

The position of the POR and the orientation of the payload for each stage of the RMS maneuver sequence are tabulated in Table X in the coordinates to be used by the RMS flight software for an auto sequence.

The joint angles and end effector positions and attitudes for the initial, final, and fly-by points for this maneuver are tabulated in Table XI.

Figures 19a through 19f, 20a through 20f, and 21a through 21f give a front, side, and top view respectively of the pictorial history of the alternate configuration panel jettison sequence.

ATTITUDE FOR PRIMARY JETTISON CONFIGURATION

PITCH	YAW	ROLL	(FROM LVLH SYSTEM)
0	270	0	

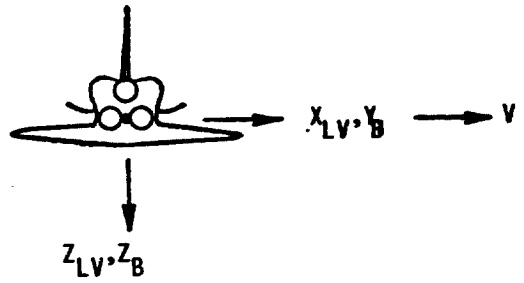

ATTITUDE FOR ALTERNATE JETTISON CONFIGURATION

PITCH	YAW	ROLL	(FROM LVLH SYSTEM)
90	0	90	

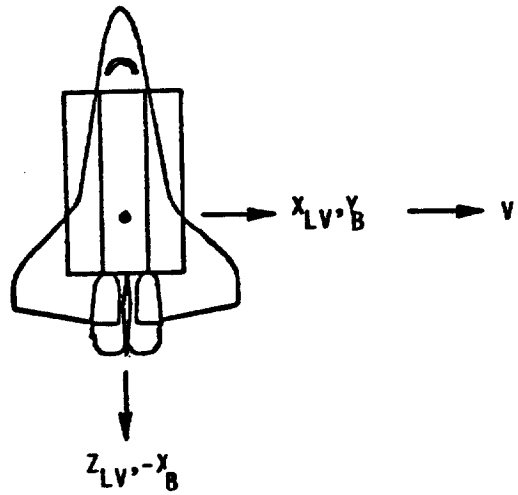

Fig. 11

ORBITER ATTITUDES

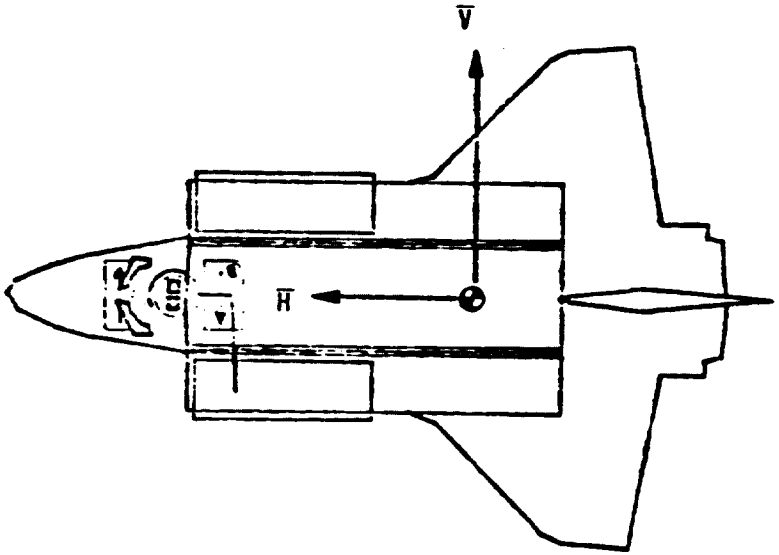

Fig. 12

PRIMARY JETTISON CONFIGURATION

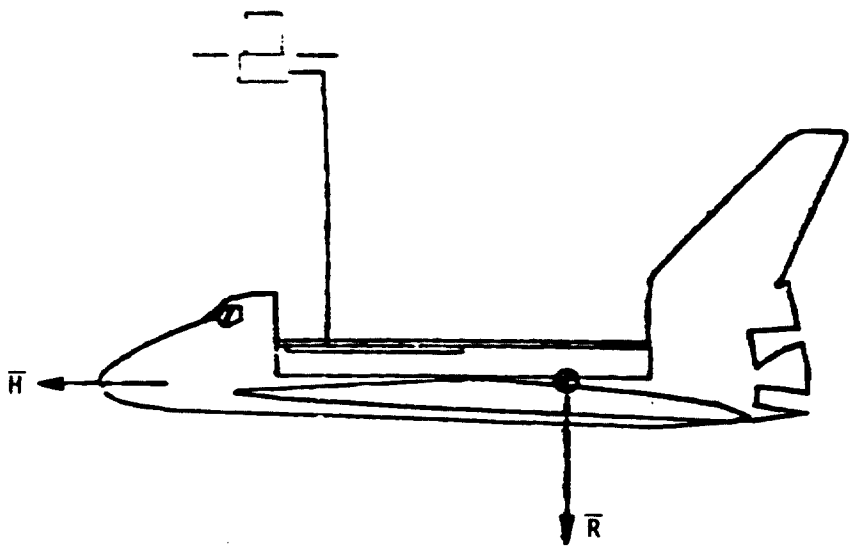

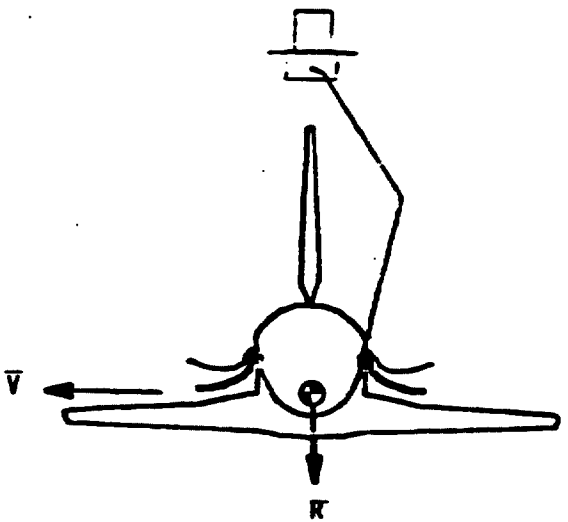

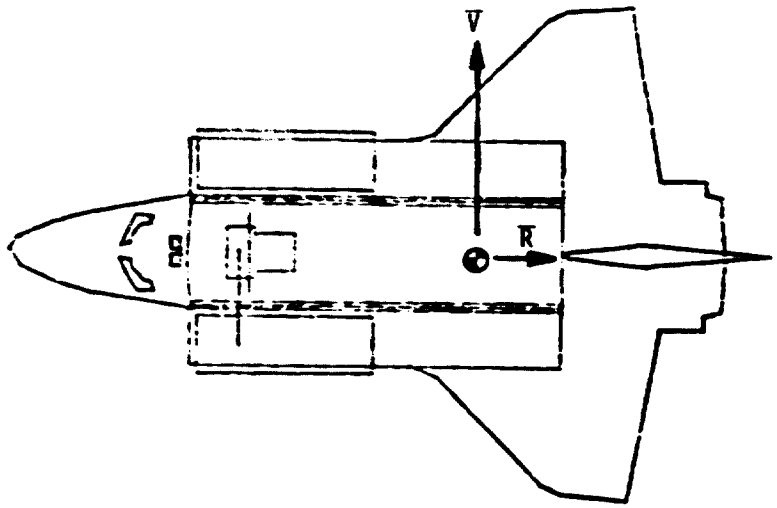

Fig. 13

ALTERNATE JETTISON CONFIGURATION

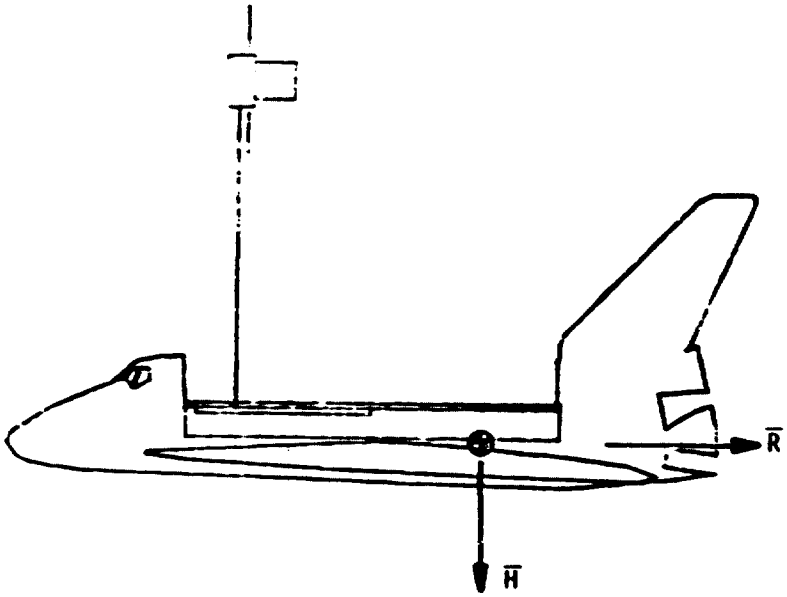

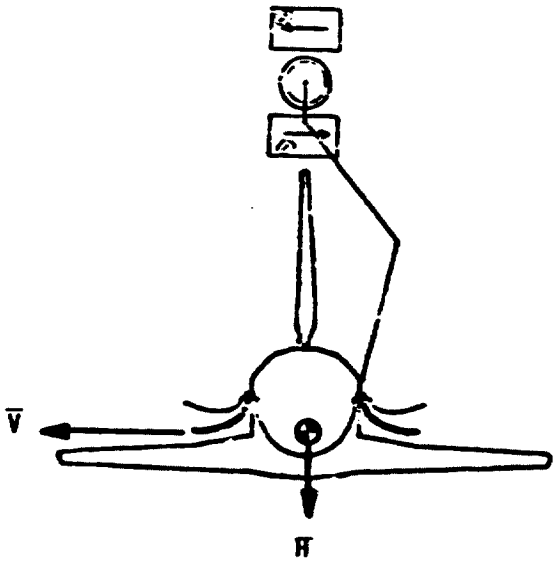

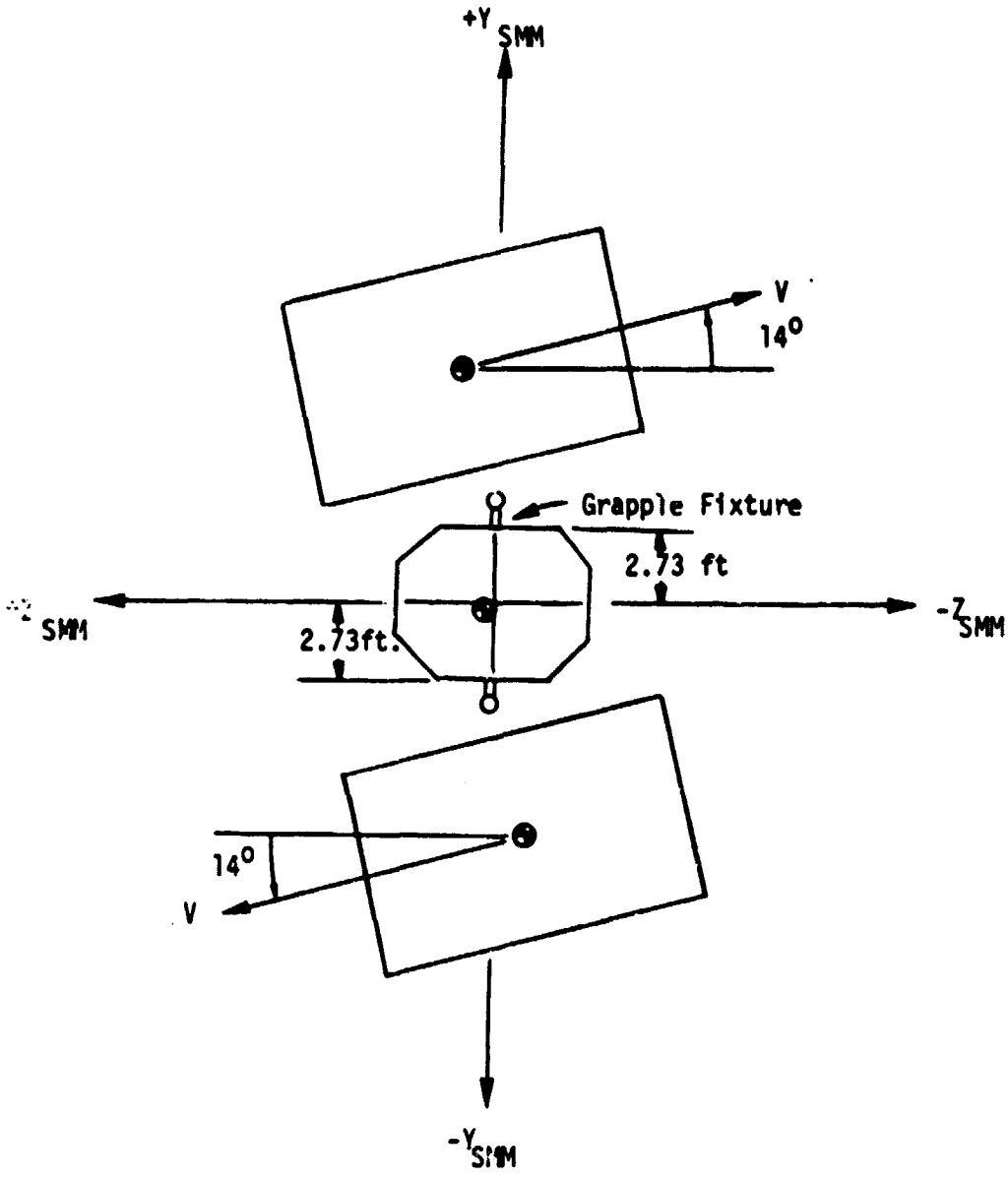

Fig. 14

SOLAR ARRAY SYSTEM JETTISON POSITION
(TOP VIEW)

TABLE IX

Primary and Alternate Jettison Configuration RMS Auto Sequences with POR in Orbiter Body Axis Coordinate System and Payload Orientation in Orbiter Rotation Axis System. (All units in inches and degrees)

POR is at origin at Payload Coordinate System

Primary Configuration RMS Maneuver Sequence			
POR - XYZ	-505.0	0.0	-926.0
PL - PYR	90	0	76
	0	284	0
	270	0	284
	270	0	256

Alternate Configuration RMS Maneuver Sequence			
POR - XYZ	-692.0	0.0	-950.0
PL - PYR	0	0	76
	270	284	0
	180	0	284
	180	0	256

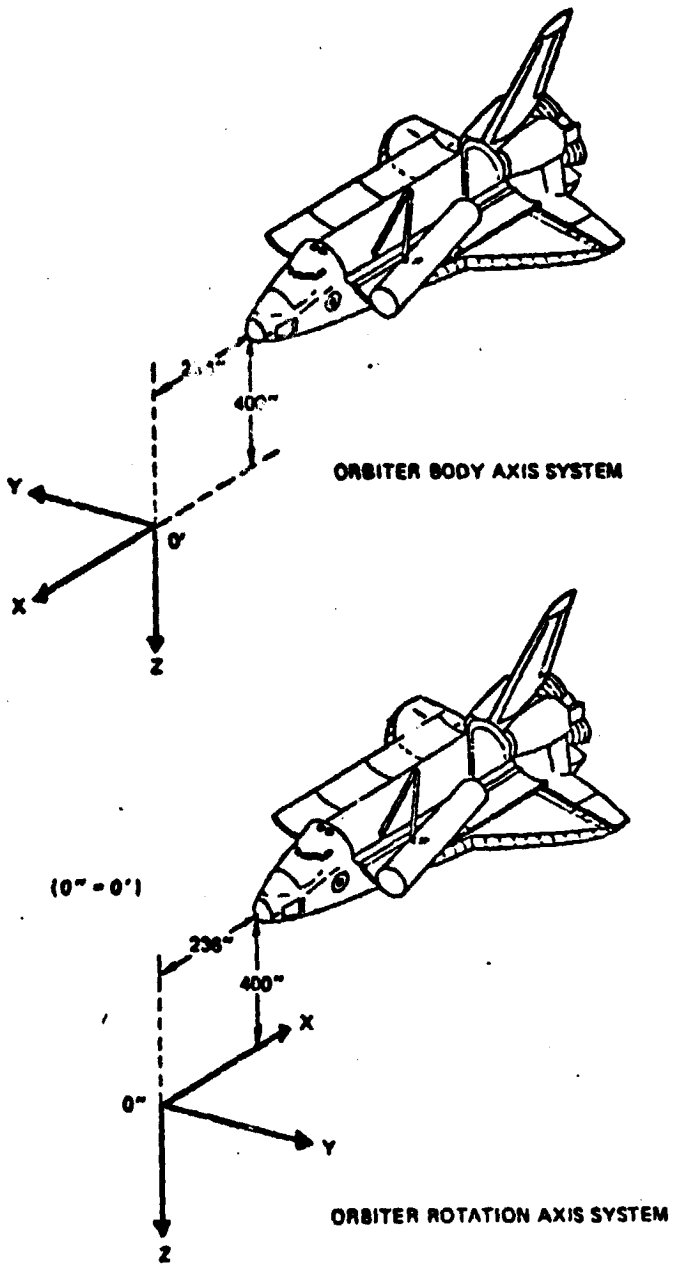

Fig. 15

RELATIONSHIP BETWEEN ORBITER BODY AXIS SYSTEM

AND ORBITER ROTATION AXIS SYSTEM

TABLE X

PRIMARY JETTISON CONFIGURATION RMS MANEUVER

Initial Configuration

See Figs. 16a, 16b, 17a, 17b, 18a, 18b

POR-XYZ	-14.50	8.00	43.00
EE-XYZ	-11.85	7.34	43.00
ee-rpy	0.00	0.00	166.00
roll out angle		19.48	

angle	x	y	z	
shy	109.9857	0.0000	-8.3193	1.0901
shp	-85.5486	0.0000	-0.7769	2.7096
elp	47.0412	-0.7254	-6.0216	33.1921
wrp	46.9129	-6.8147	4.8230	42.7420
wry	56.5025	-7.3219	6.2168	43.0003
wrr	11.9184	-11.8500	7.3398	43.0003

First Fly-by Point

See Figs. 16c, 17c, 18c

EE-XYZ	-11.85	7.34	43.00
ee-rpy	90.00	0.00	166.00
roll out angle		19.48	

angle	x	y	z	
shy	109.9857	0.0000	-8.3193	1.0901
shp	-85.5486	0.0000	-0.7769	2.7096
elp	47.0412	-0.7254	-6.0216	33.1921
wrp	46.9129	-6.8147	4.8230	42.7420
wry	56.5025	-7.3219	6.2168	43.0003
wrr	101.9184	-11.8500	7.3398	43.0003

Second Fly-by Point

See Figs. 16d, 17d, 18d

EE-XYZ	-11.85	7.34	43.00
ee-rpy	180.00	0.00	166.00
roll out angle		19.48	

angle	x	y	z	
shy	109.9857	0.0000	-8.3193	1.0901
shp	-85.5486	0.0000	-0.7769	2.7096
elp	47.0412	-0.7254	-6.0216	33.1921
wrp	46.9129	-6.8147	4.8230	42.7420
wry	56.5025	-7.3219	6.2168	43.0003
wrr	-168.0816	-11.8500	7.3398	43.0003

Final Configuration

See Figs. 16e, 16f, 17e, 17f, 18e, 18f

EE-XYZ	-11.85	8.66	43.00
ee-rpy	180.00	0.00	-166.00
roll out angle		19.48	

angle	x	y	z	
shy	107.3017	0.0000	-8.3193	1.0901
shp	-79.8577	0.0000	-0.7769	2.7096
elp	48.1803	-1.2422	-4.0362	33.5616
wrp	-17.0548	-7.0276	9.2740	41.6225
wry	83.8376	-7.3219	9.7868	43.0003
wrr	-112.4973	-11.8500	8.6598	43.0003

Coordinate System Aligned With Orbiter Structural Reference System With Origin At Shoulder Attach Point

All Units In Feet And Degrees

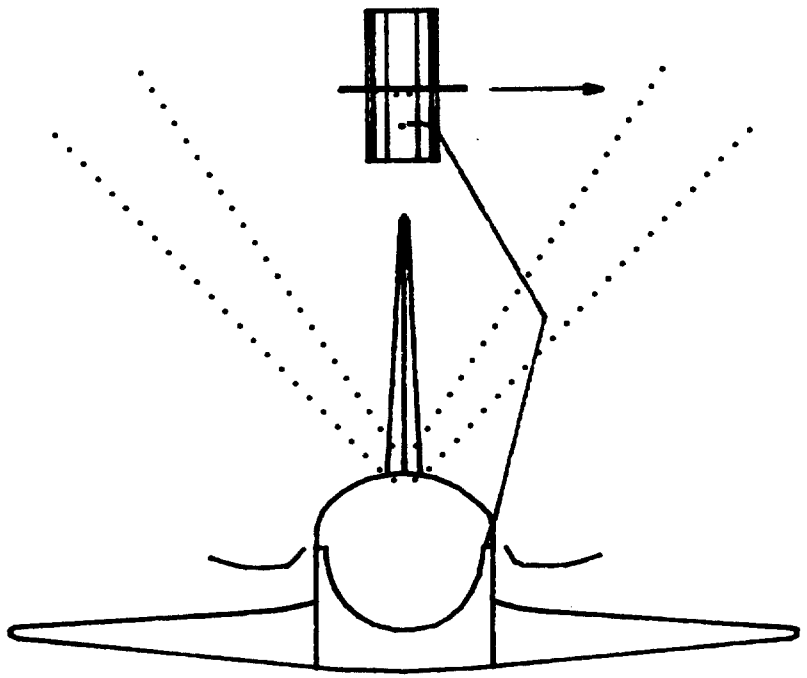

Figs. 16a thru 16f

PRIMARY JETTISON CONFIGURATION SEQUENCE
Front View

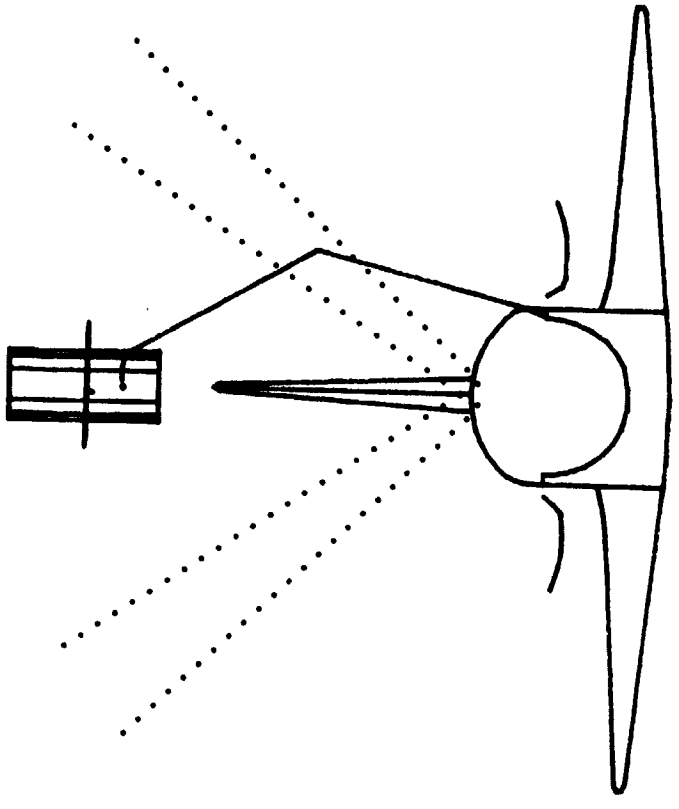

Fig. 16b

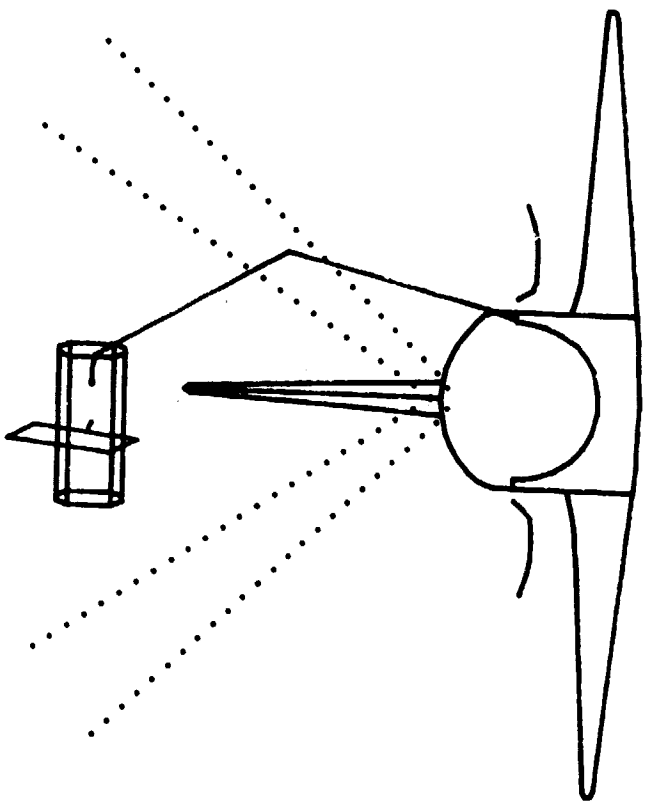

Fig. 16c

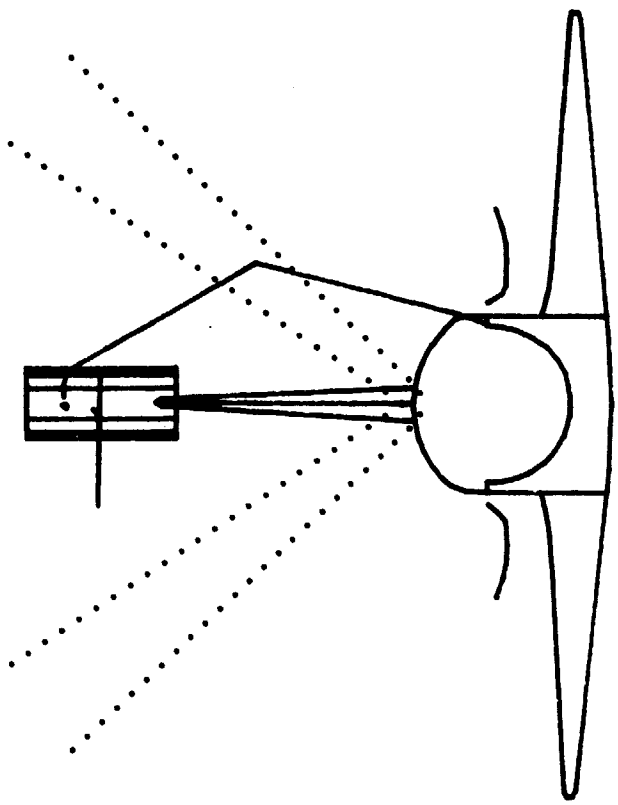

Fig. 16d

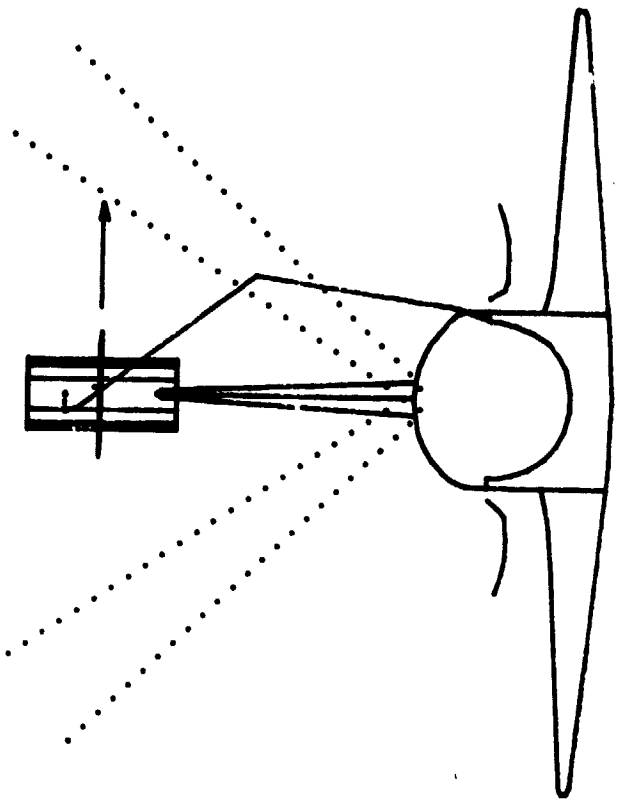

Fig. 16e

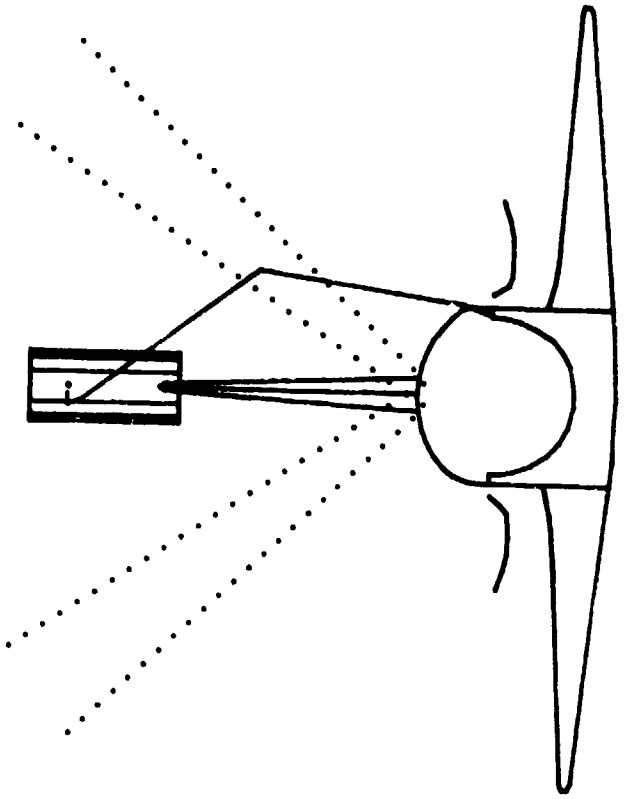

Fig. 16f

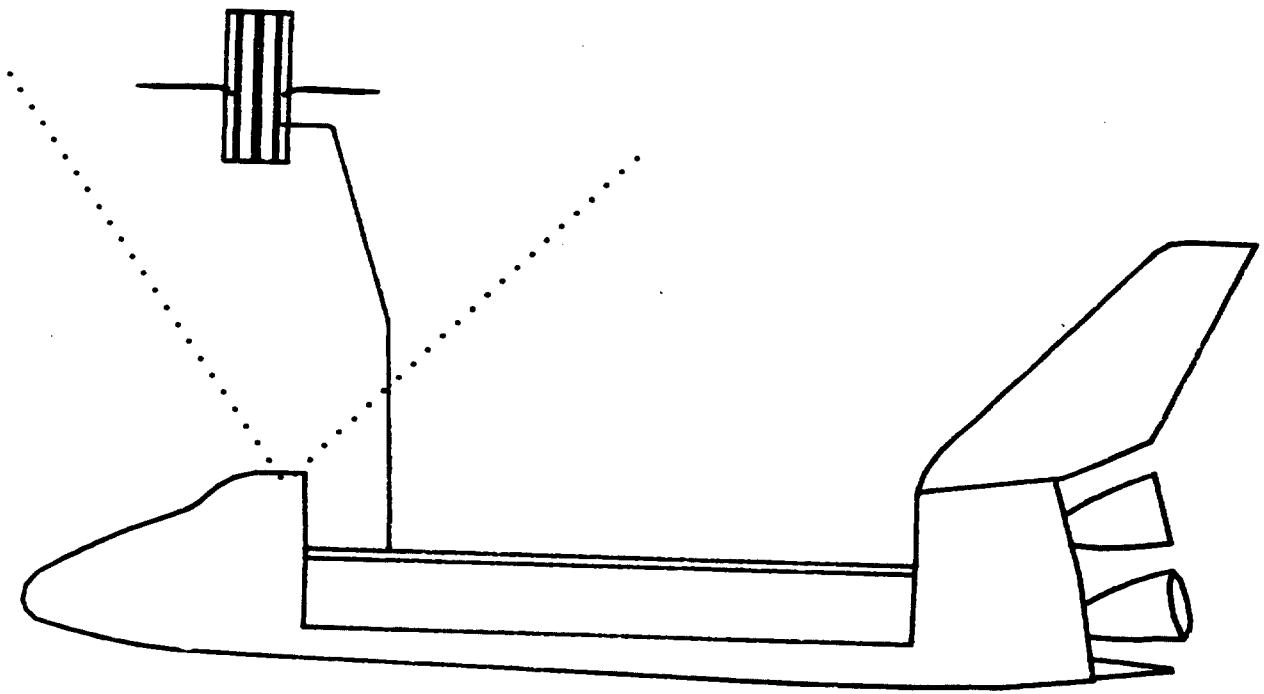

Figs. 17a thru 17f

PRIMARY JETTISON CONFIGURATION SEQUENCE
Side View

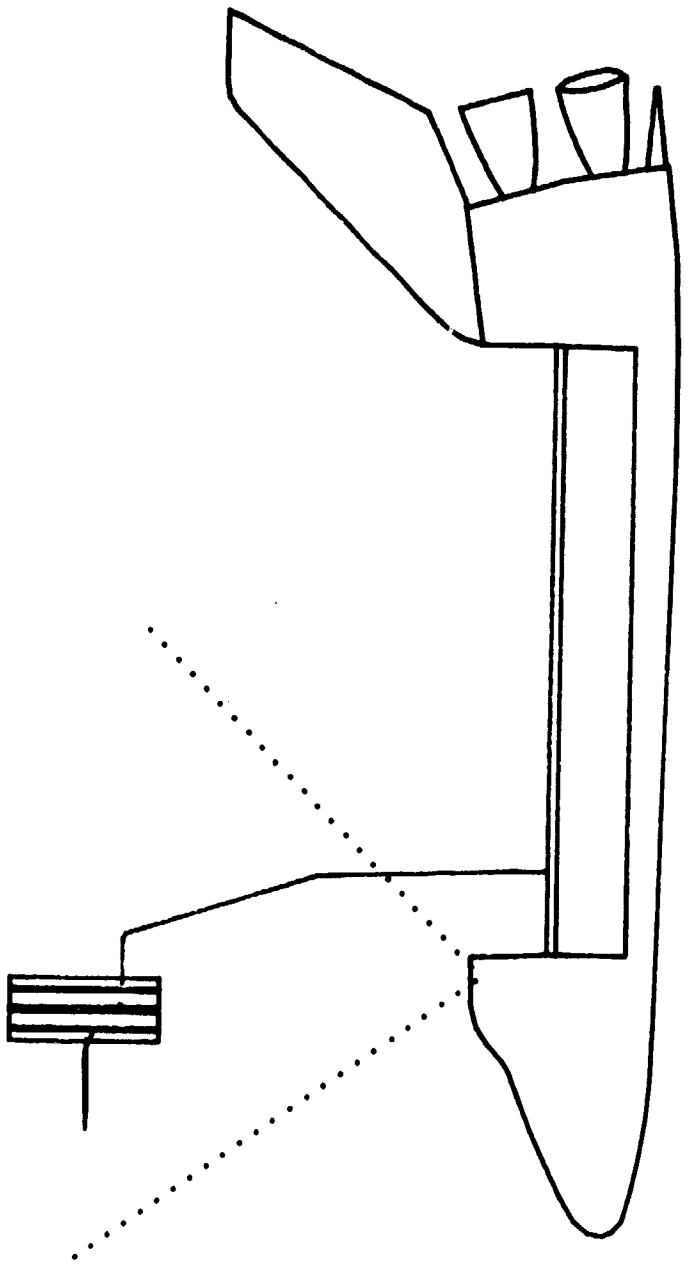

Fig. 17b

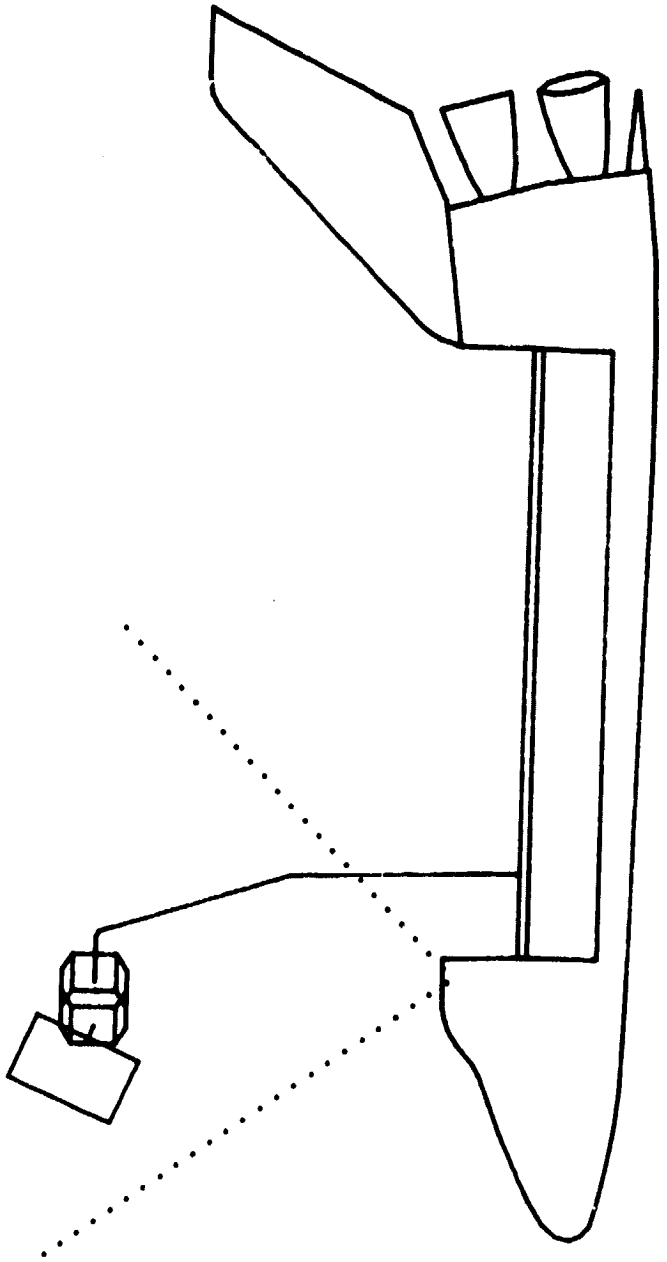

Fig. 17c

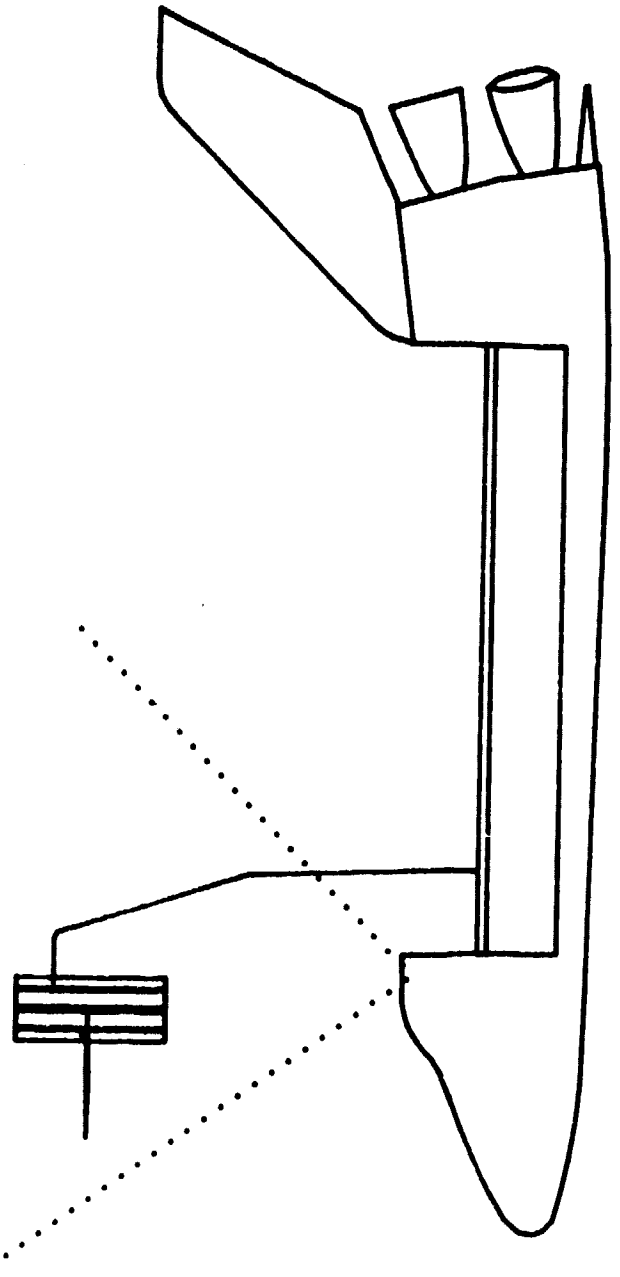

Fig. 17d

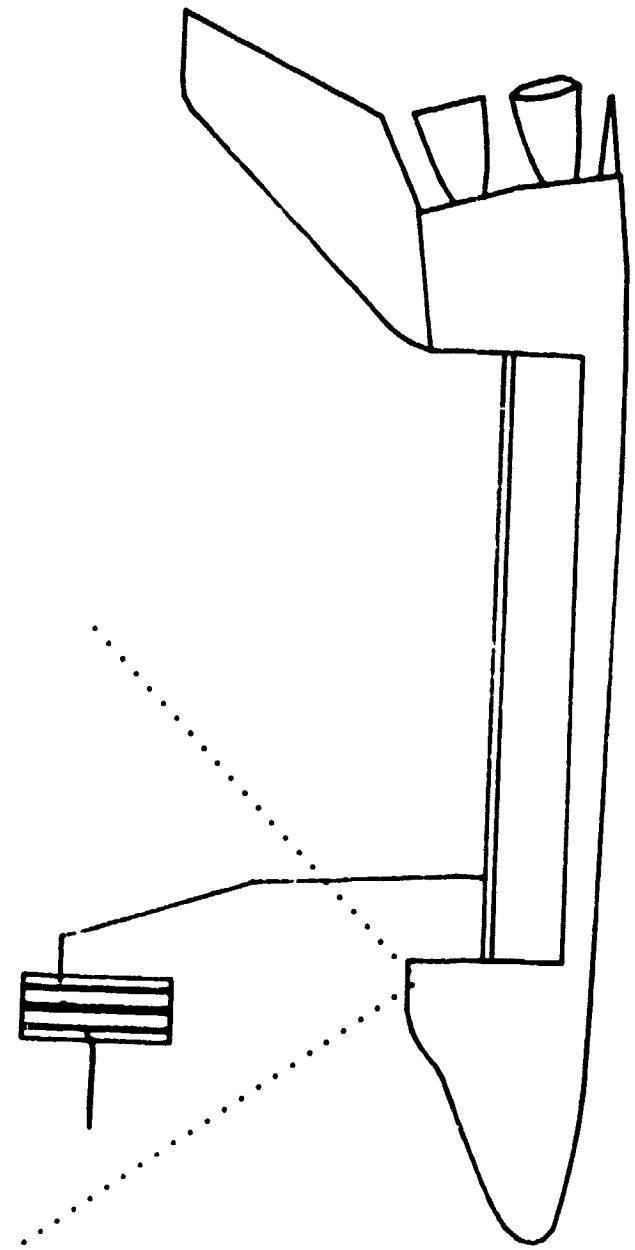

Fig. 17e

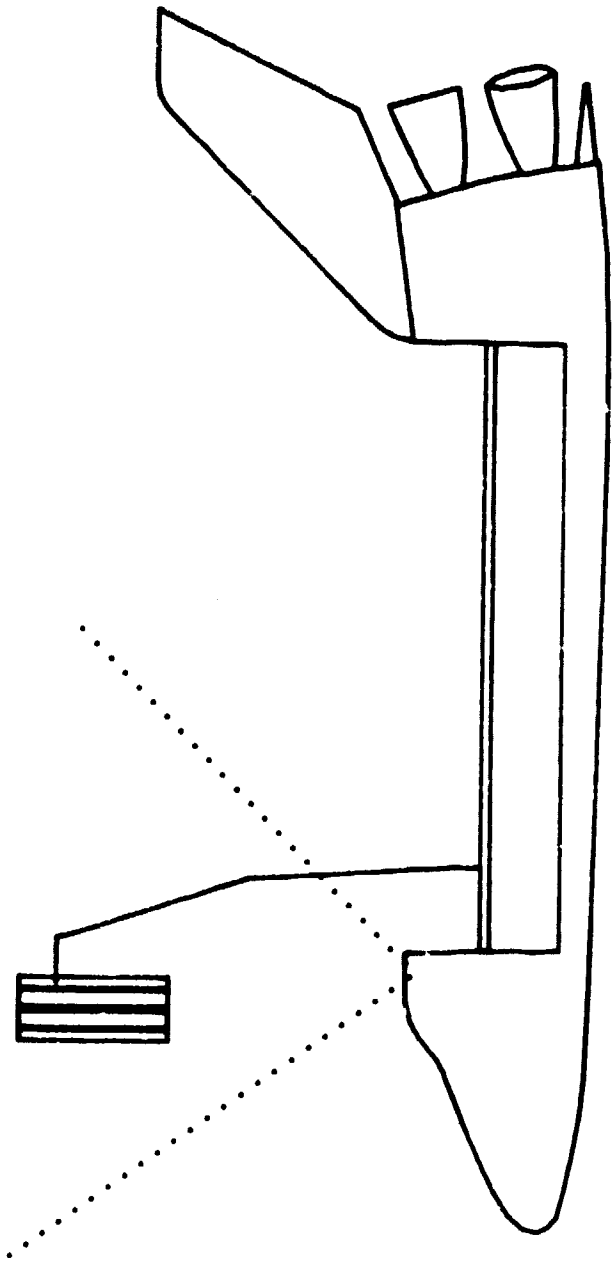

Fig. 17f

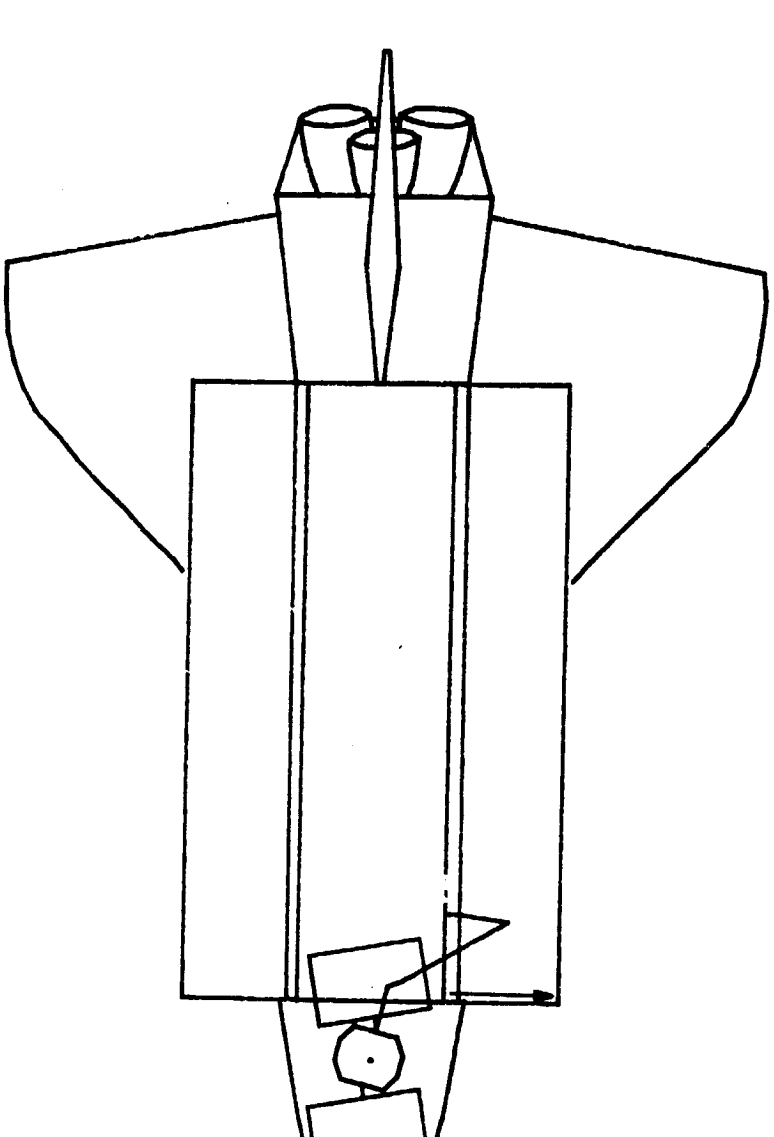

Figs. 18a thru 18f

PRIMARY JETTISON CONFIGURATION SEQUENCE
Top View

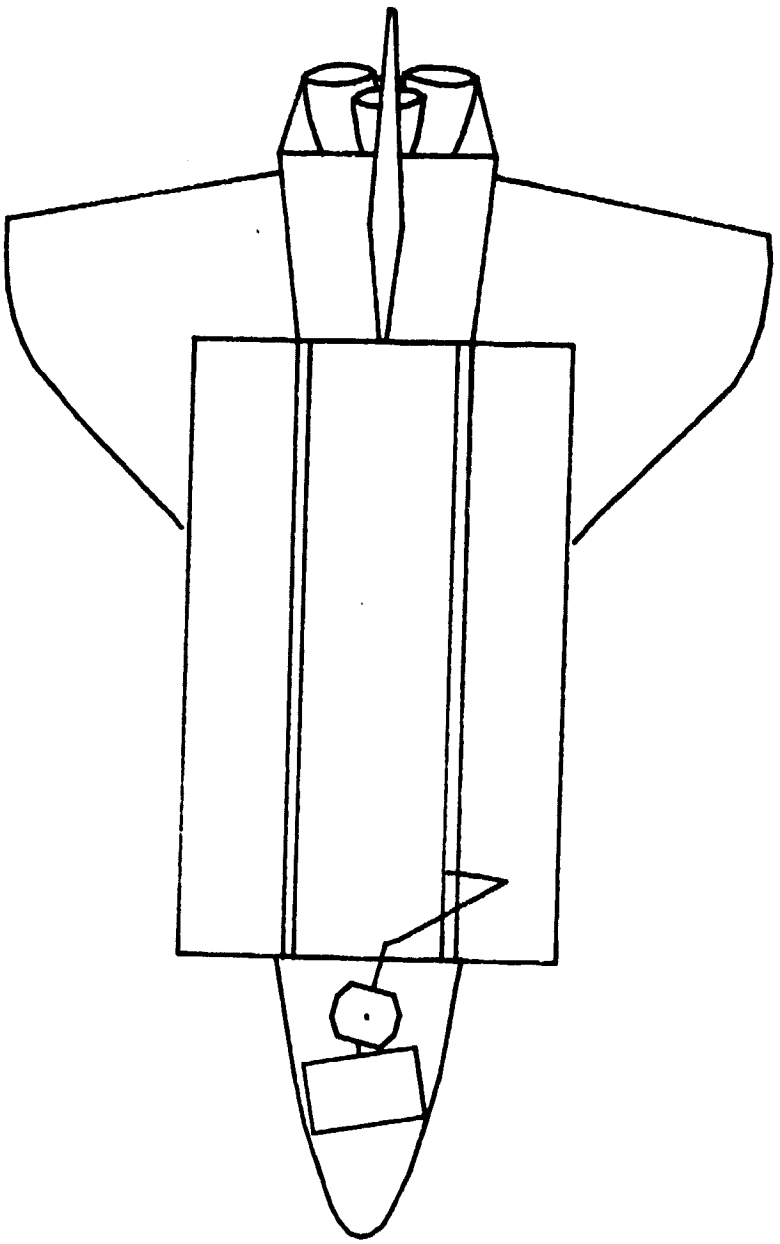

Fig. 18b

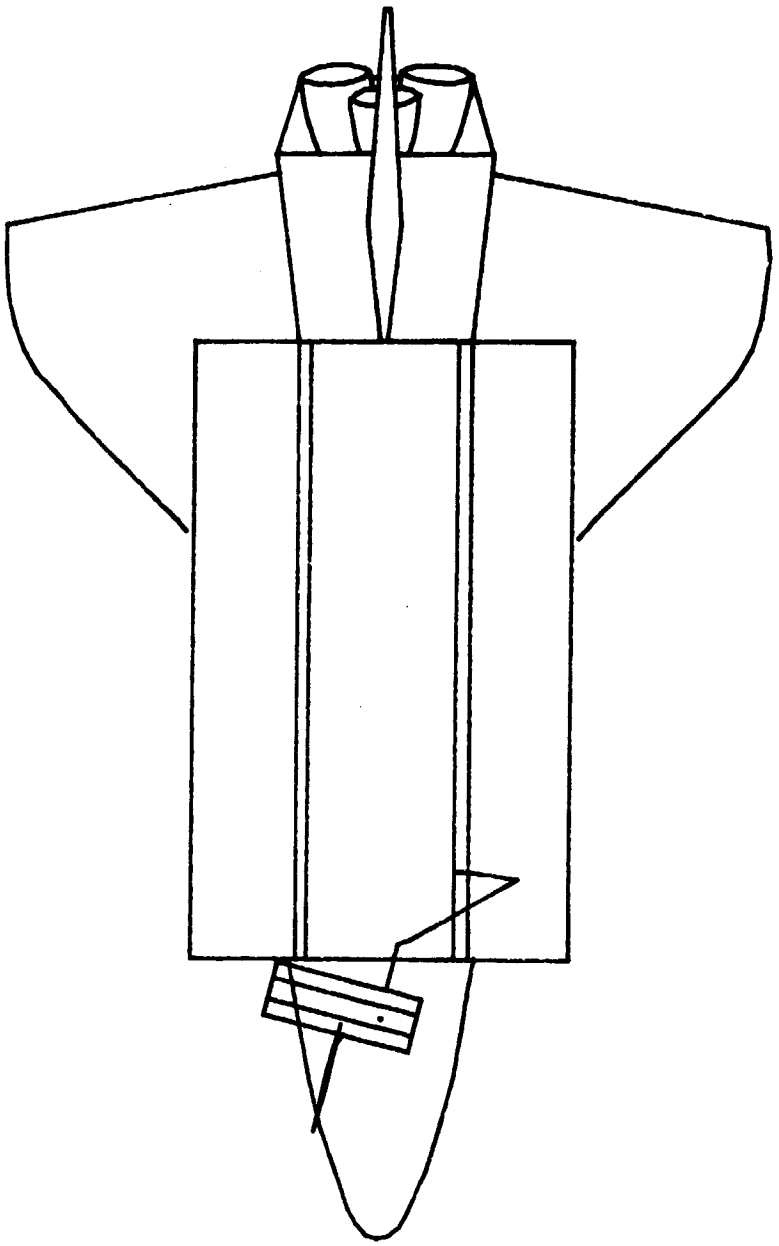

Fig. 18c

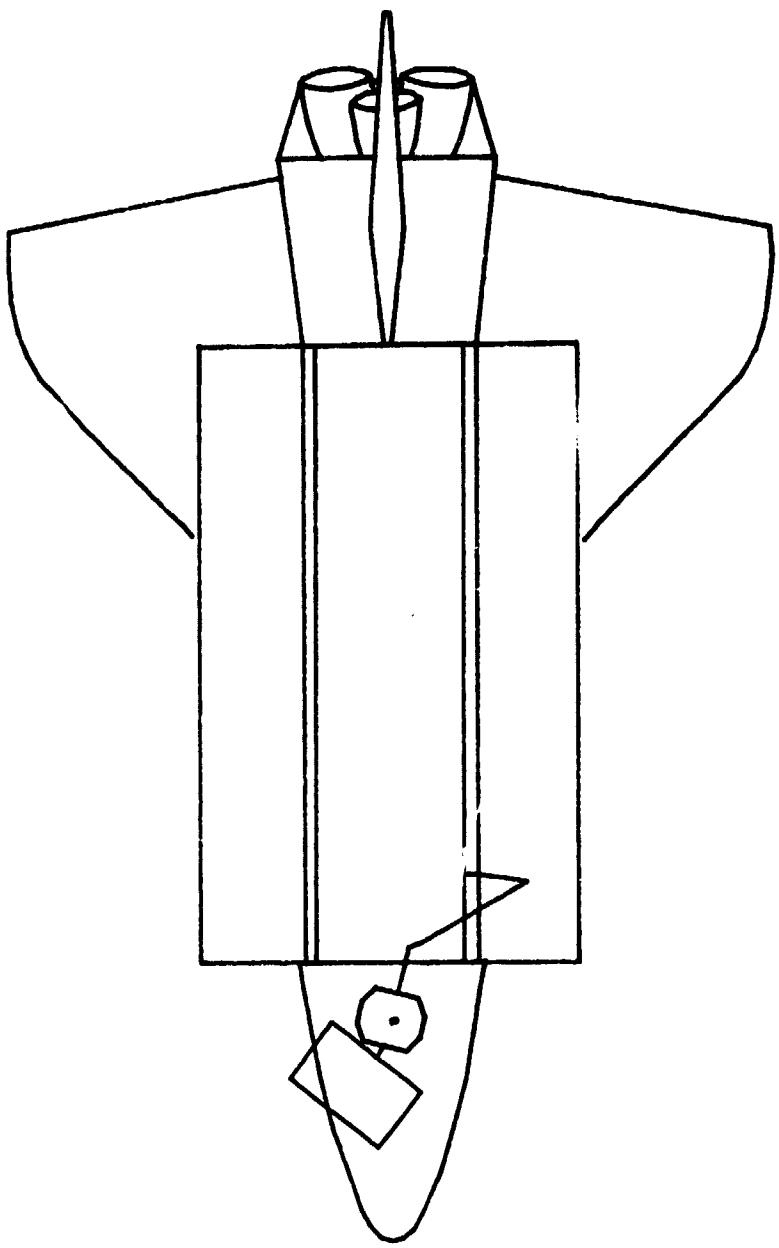

Fig. 18d

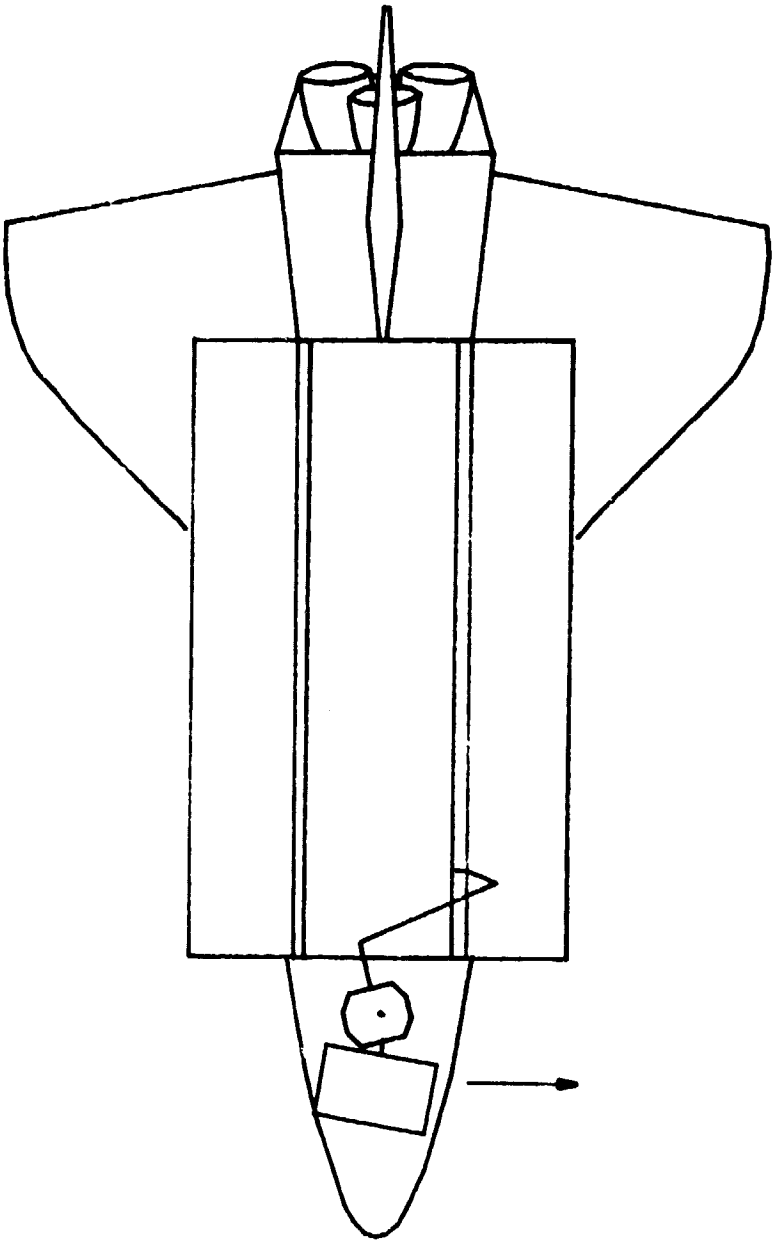

Fig. 18e

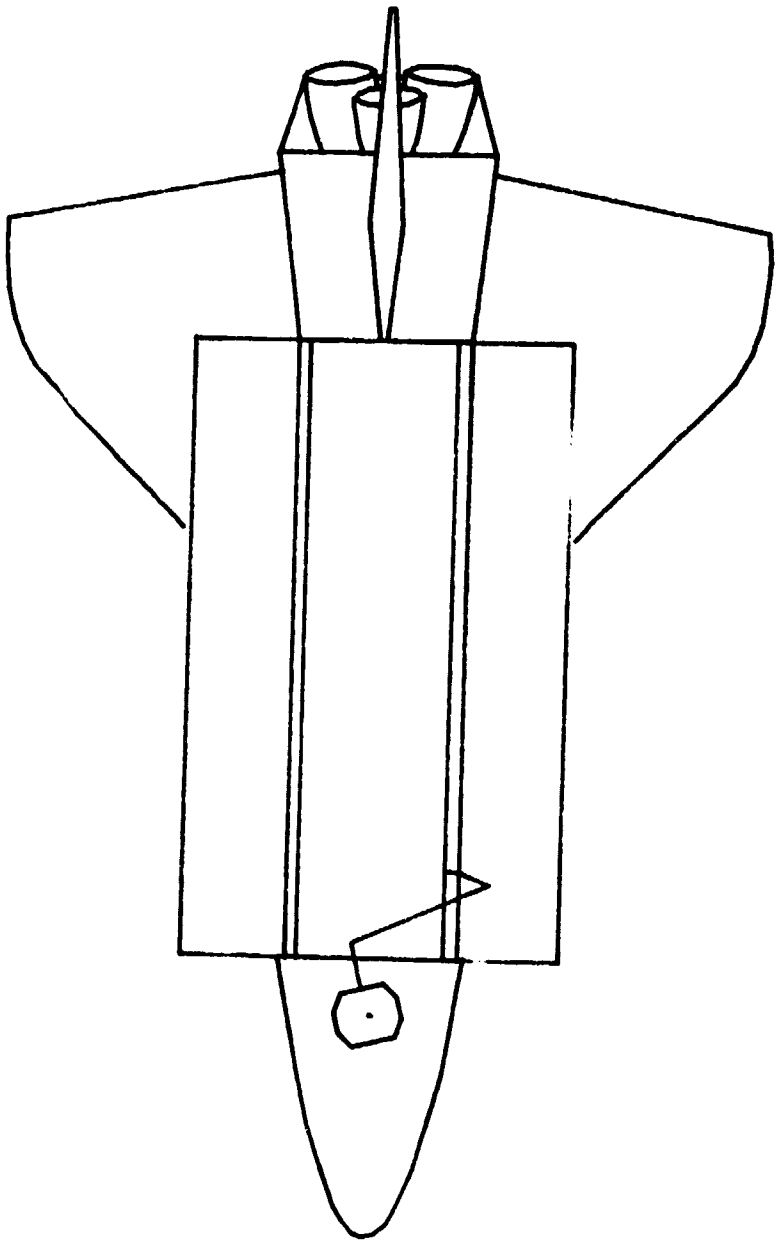

Fig. 18f

TABLE XI

ALTERNATE JETTISON CONFIGURATION RMS MANEUVER

Initial Configuration

See Figs. 19a, 19b, 20a, 20b, 21a, 21b

POR-XYZ		1.00	8.00	45.00
EE-XYZ		1.00	7.34	42.35
ee-rpy		90.00	-76.00	90.00
	roll out angle		19.48	
	angle	x	y	z
shy	86.8901	0.0000	-0.3193	1.0901
shp	-102.0076	0.0000	-0.7769	2.7096
elp	81.1539	-0.2096	-11.4555	31.0029
wrp	-35.7051	0.9551	5.8497	36.3669
wry	1.7150	1.0000	6.2165	37.8222
wrr	92.5947	1.0000	7.3395	42.3503

First Fly-by Point

See Figs. 19c, 20c, 21c

EE-XYZ		1.00	7.34	42.35
ee-rpy		180.00	-76.00	90.00
	roll out angle		19.48	
	angle	x	y	z
shy	86.8901	0.0000	-0.3193	1.0901
shp	-102.0076	0.0000	-0.7769	2.7096
elp	81.1539	-0.2096	-11.4555	31.0029
wrp	-35.7051	0.9551	5.8497	36.3669
wry	1.7150	1.0000	6.2165	37.8222
wrr	-177.4053	1.0000	7.3395	42.3503

Second Fly-by Point

See Figs. 19d, 20d, 21d

EE-XYZ		1.00	7.34	42.35
ee-rpy		-90.00	-76.00	90.00
	roll out angle		19.48	
	angle	x	y	z
shy	86.8901	0.0000	-0.3193	1.0901
shp	-102.0076	0.0000	-0.7769	2.7096
elp	81.1539	-0.2096	-11.4555	31.0029
wrp	-35.7051	0.9551	5.8497	36.3669
wry	1.7150	1.0000	6.2165	37.8222
wrr	-87.4053	1.0000	7.3395	42.3503

Final Configuration

See Figs. 19e, 19f, 20e, 20f, 21e, 21f

EE-XYZ		1.00	8.66	42.35
ee-rpy		90.00	-76.00	-90.00
	roll out angle		19.48	
	angle	x	y	z
shy	87.3711	0.0000	-0.3193	1.0901
shp	-92.6104	0.0000	-0.7769	2.7096
elp	76.4592	-0.0208	-8.3035	32.4730
wrp	-68.3745	0.9934	10.1517	36.3669
wry	0.2510	1.0000	9.7885	37.8223
wrr	-87.3830	1.0000	8.6595	42.3504

Coordinate System Aligned With Orbiter Structural Reference System With Origin At Shoulder Attach Point

All Units In Feet And Degrees

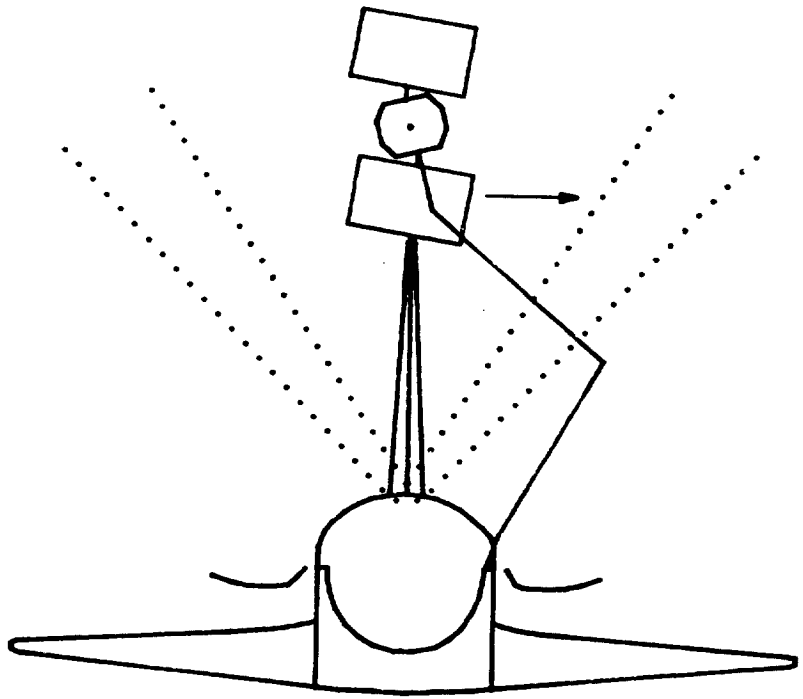

Figs. 19a thru 19f

ALTERNATE JETTISON CONFIGURATION SEQUENCE
Front View

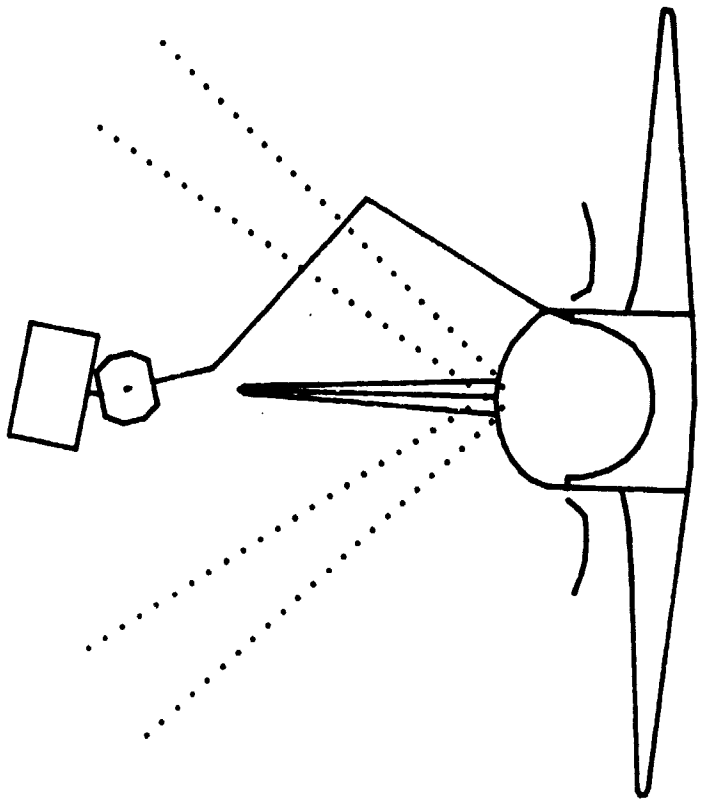

Fig. 19b

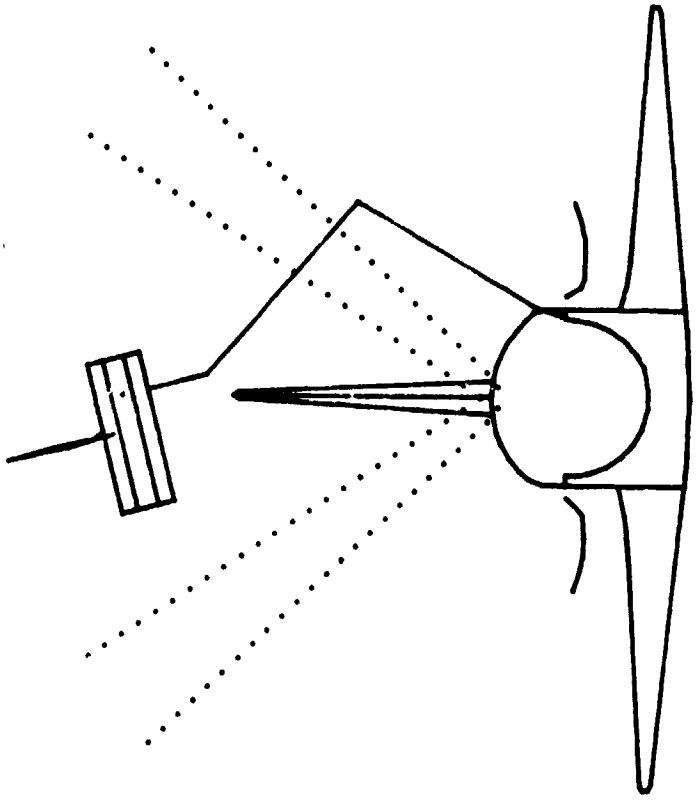

Fig. 19c

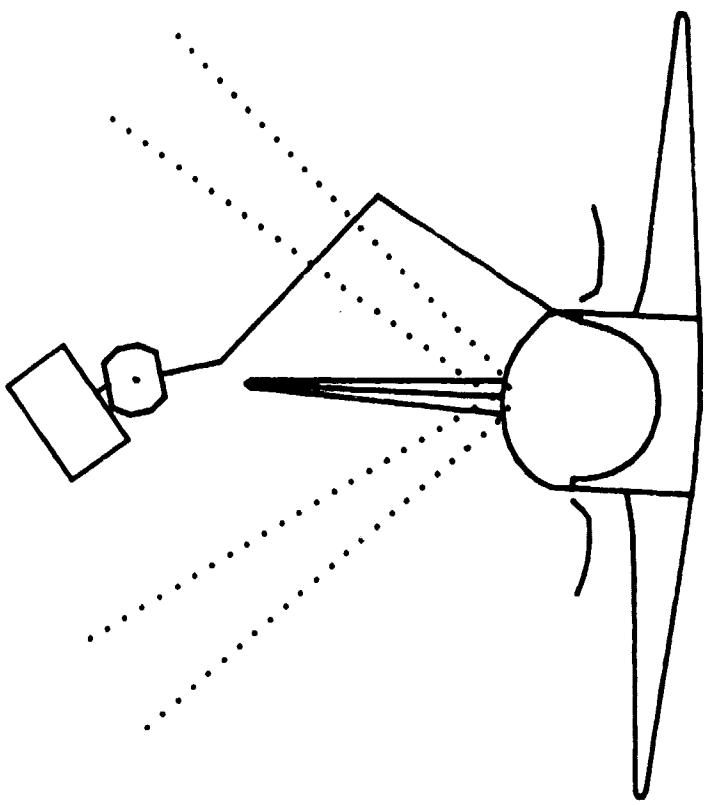

Fig. 19d

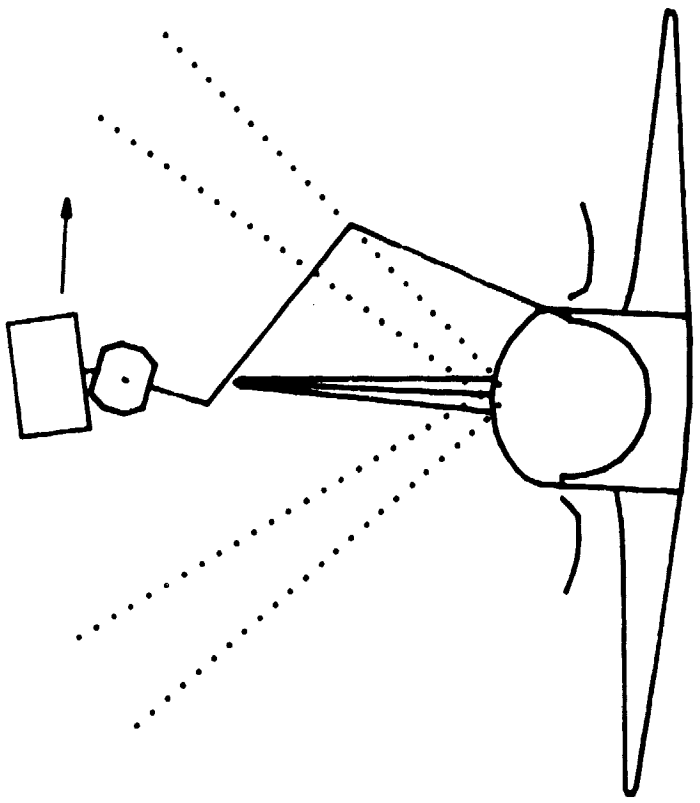

Fig. 19e

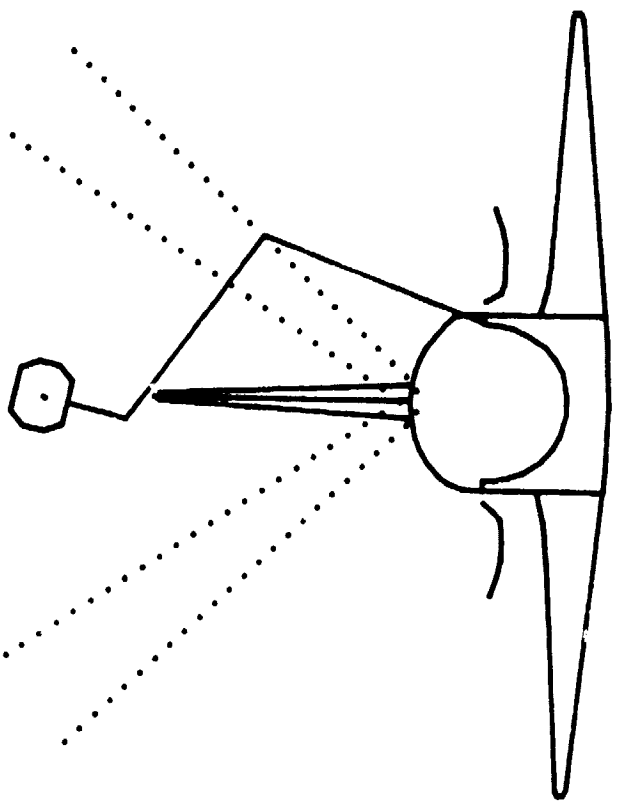

Fig. 19f

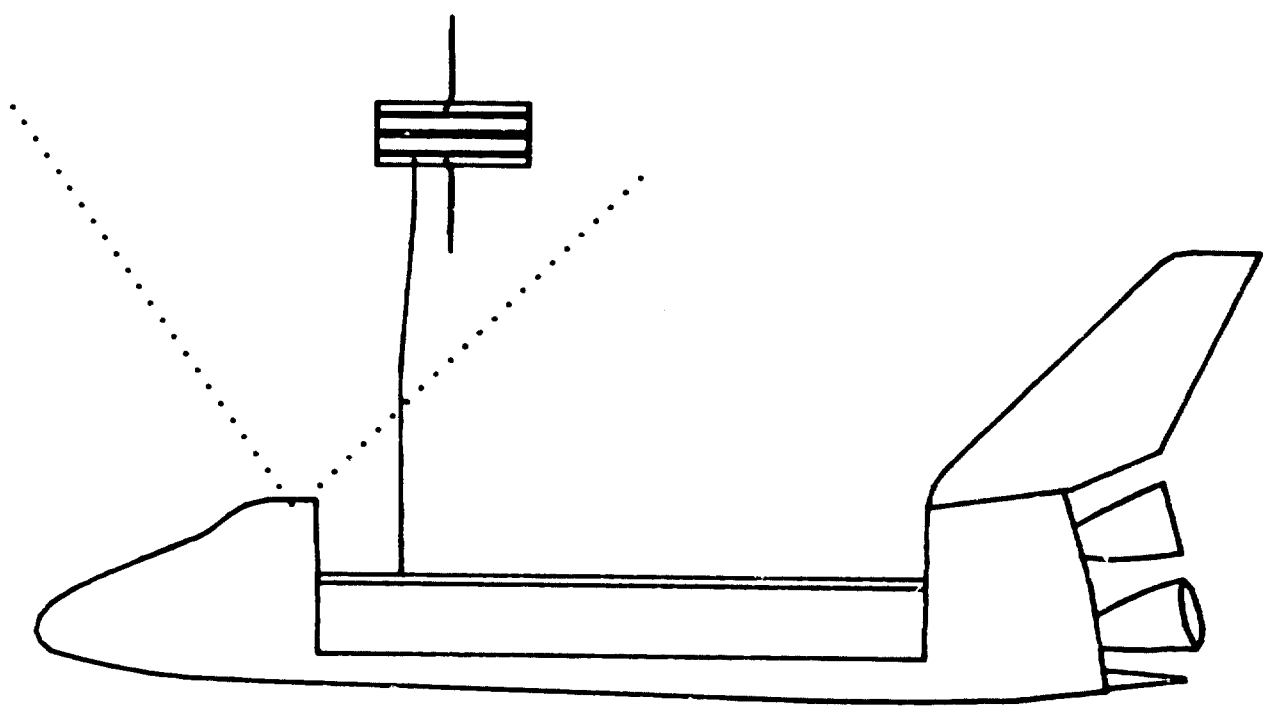

Figs. 20a thru 20f

ALTERNATE JETTISON CONFIGURATION SEQUENCE
Side View

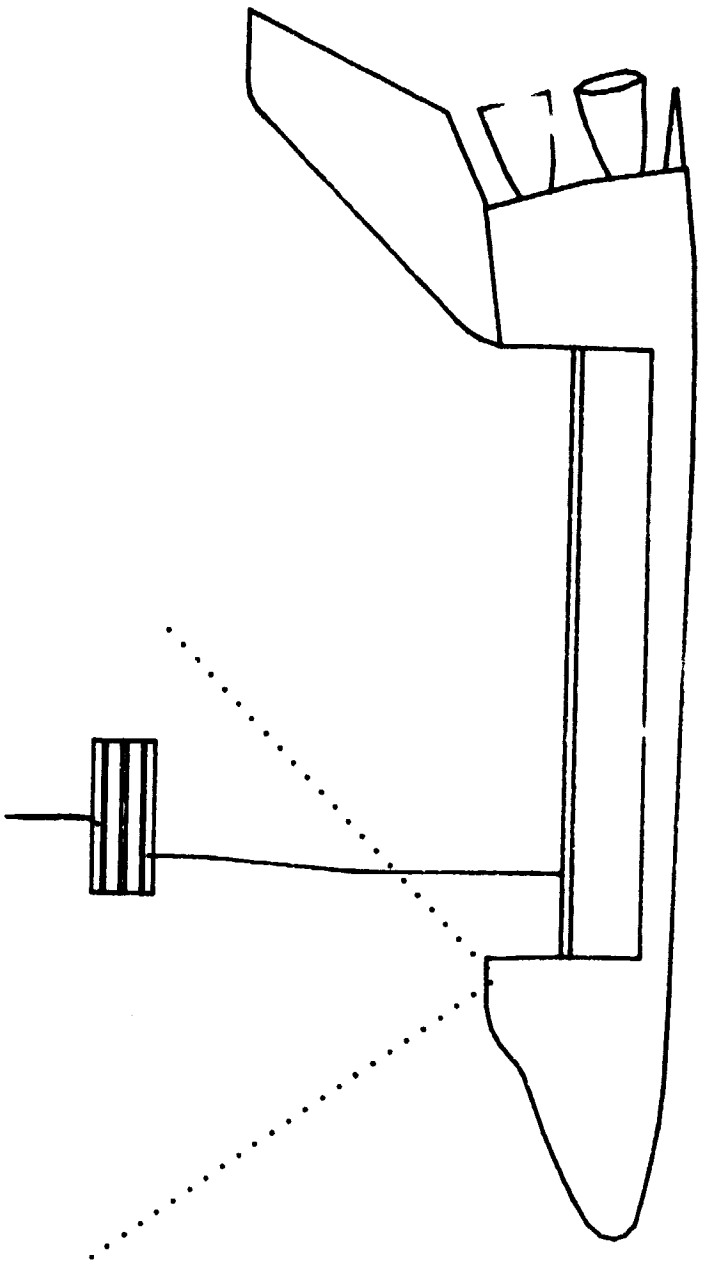

Fig. 20b

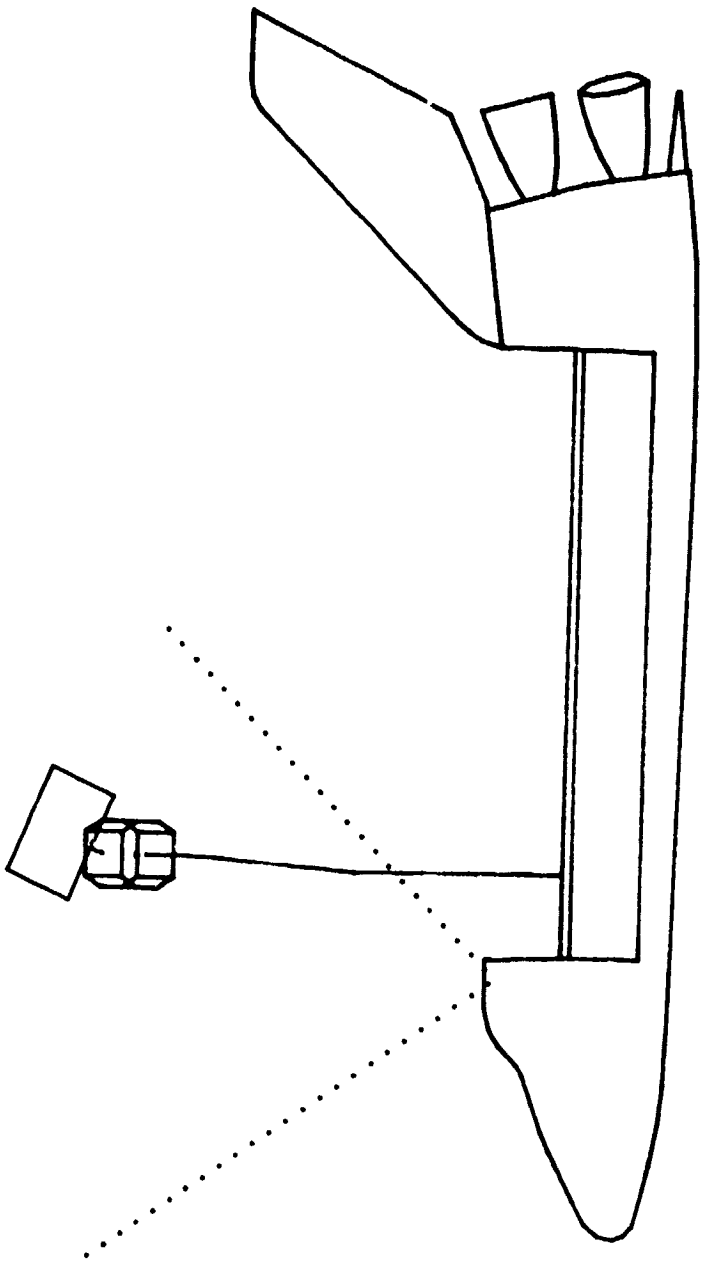

Fig. 20c

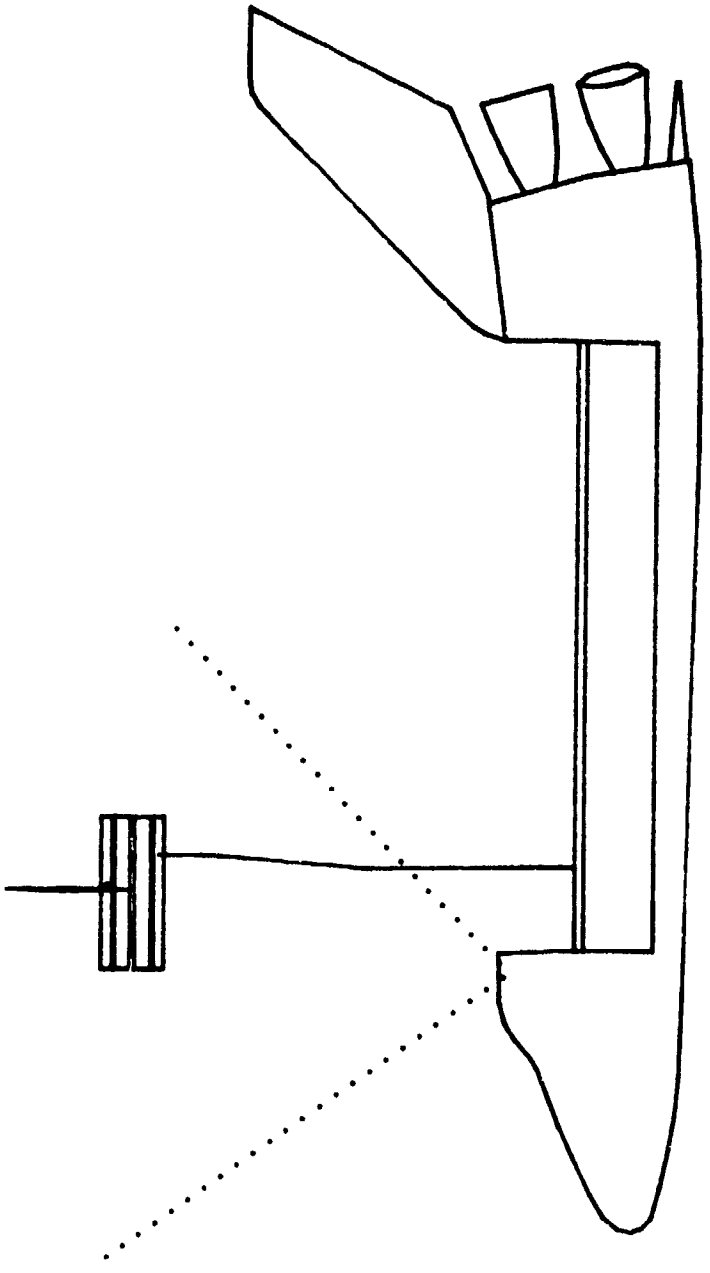

Fig. 20d

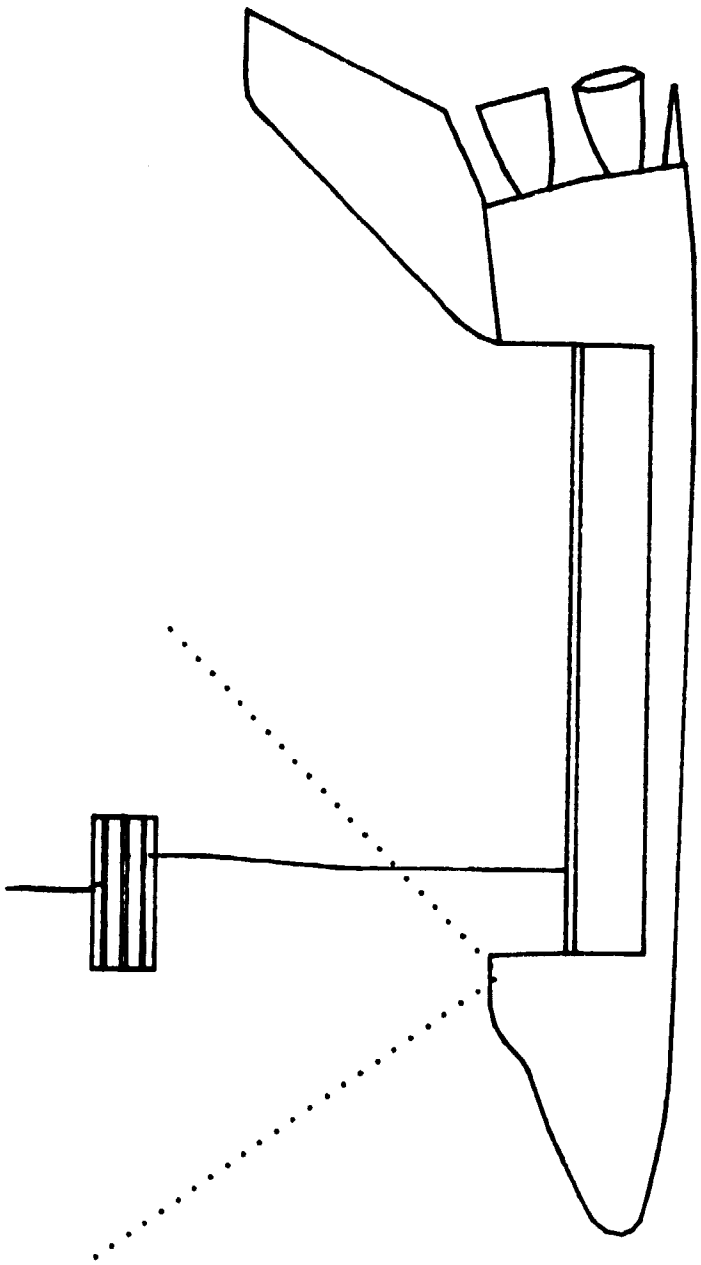

Fig. 20e

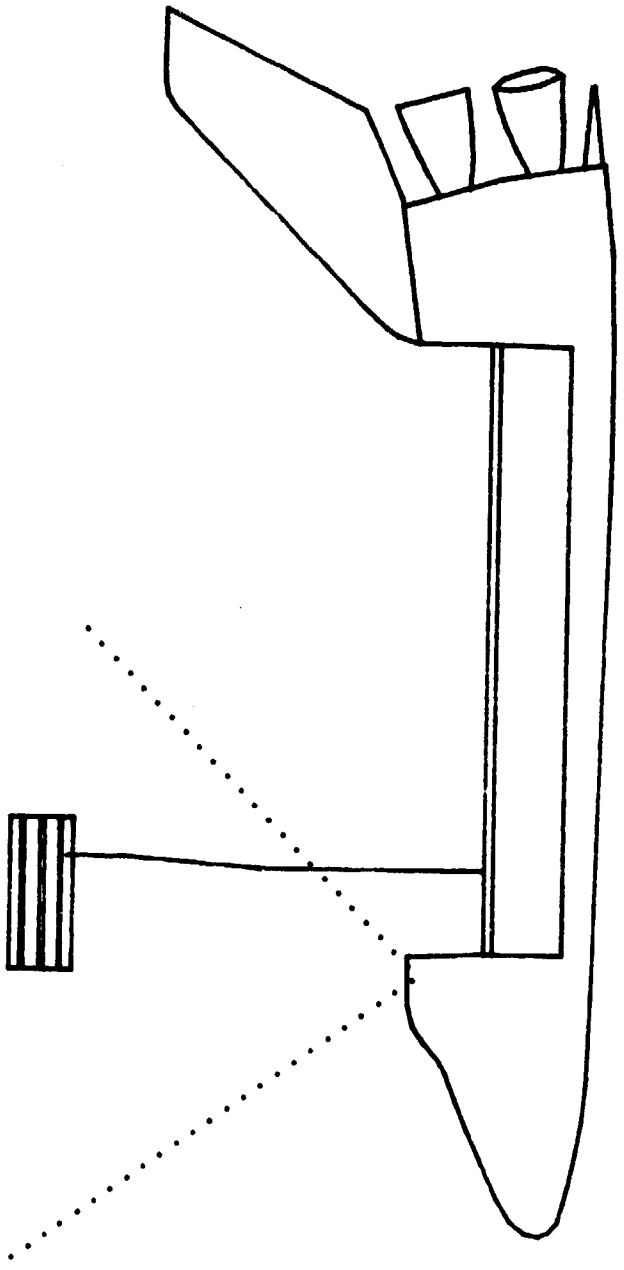

Fig. 20f

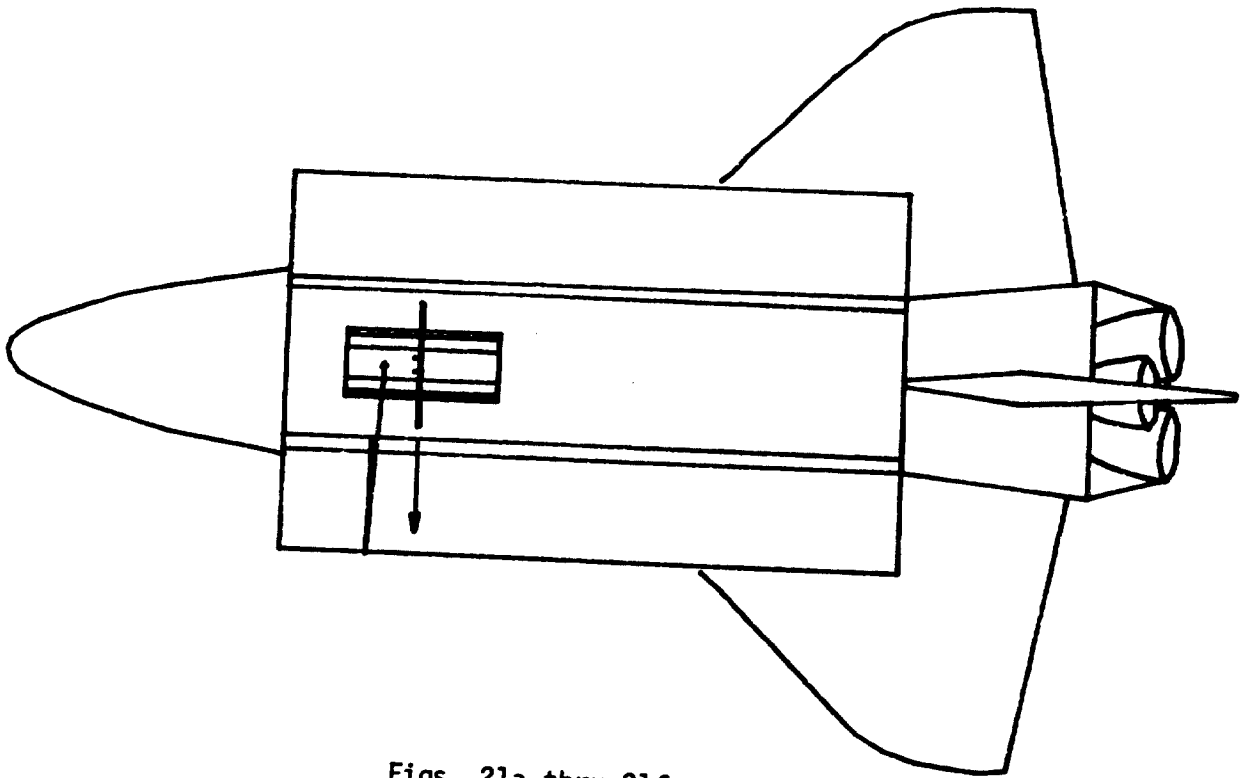

Figs. 21a thru 21f

ALTERNATE JETTISON CONFIGURATION SEQUENCE
Top View

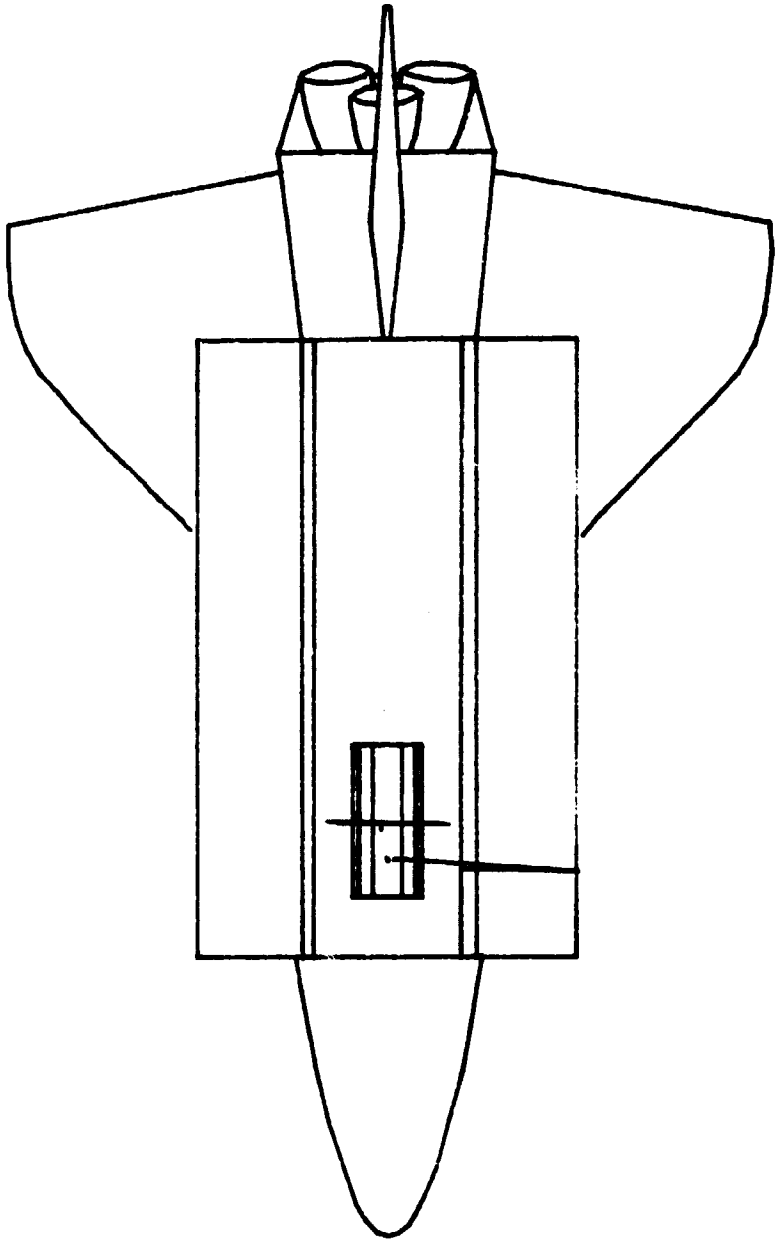

Fig. 21b

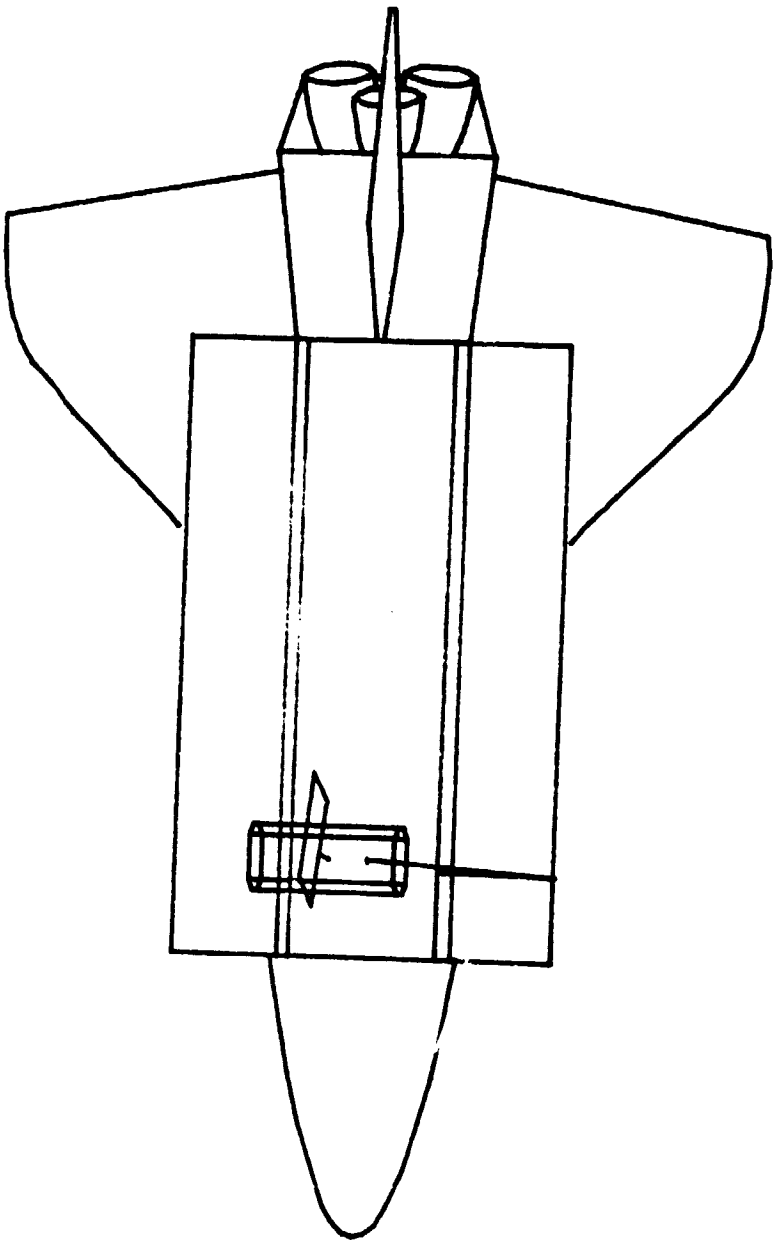

Fig. 21c

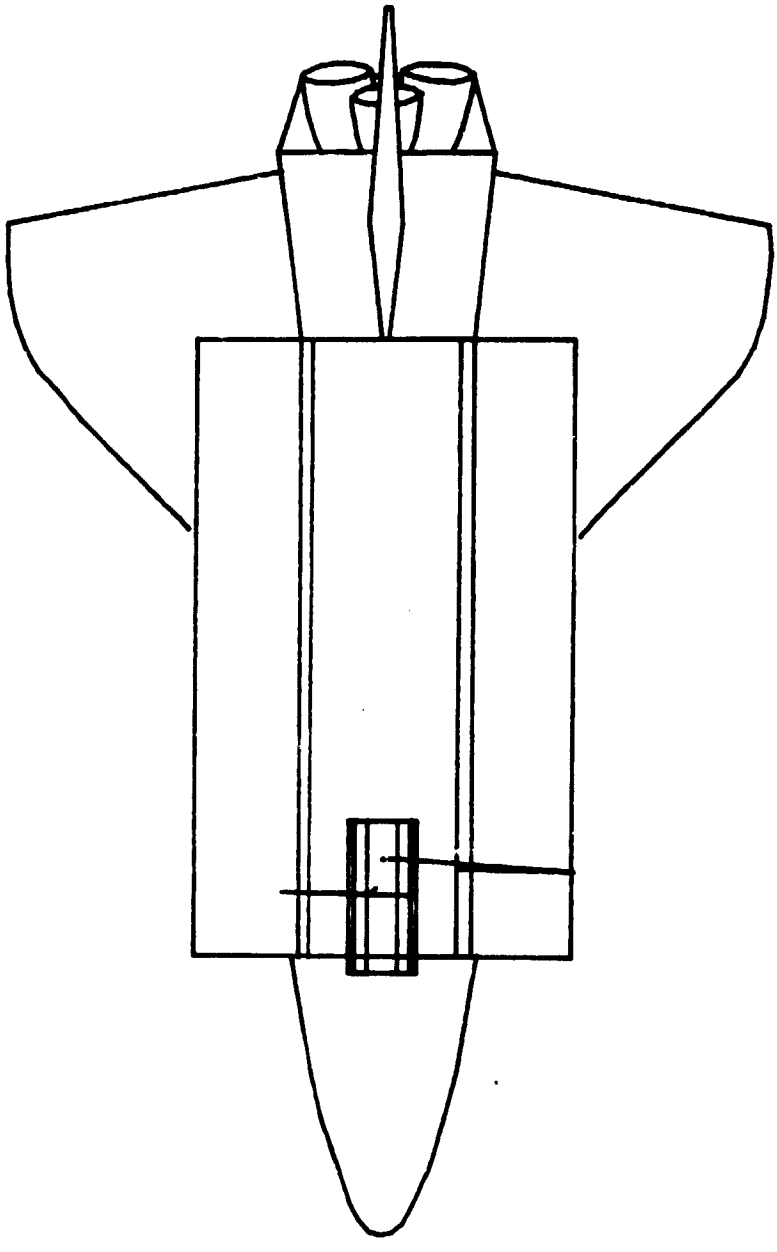

Fig. 21d

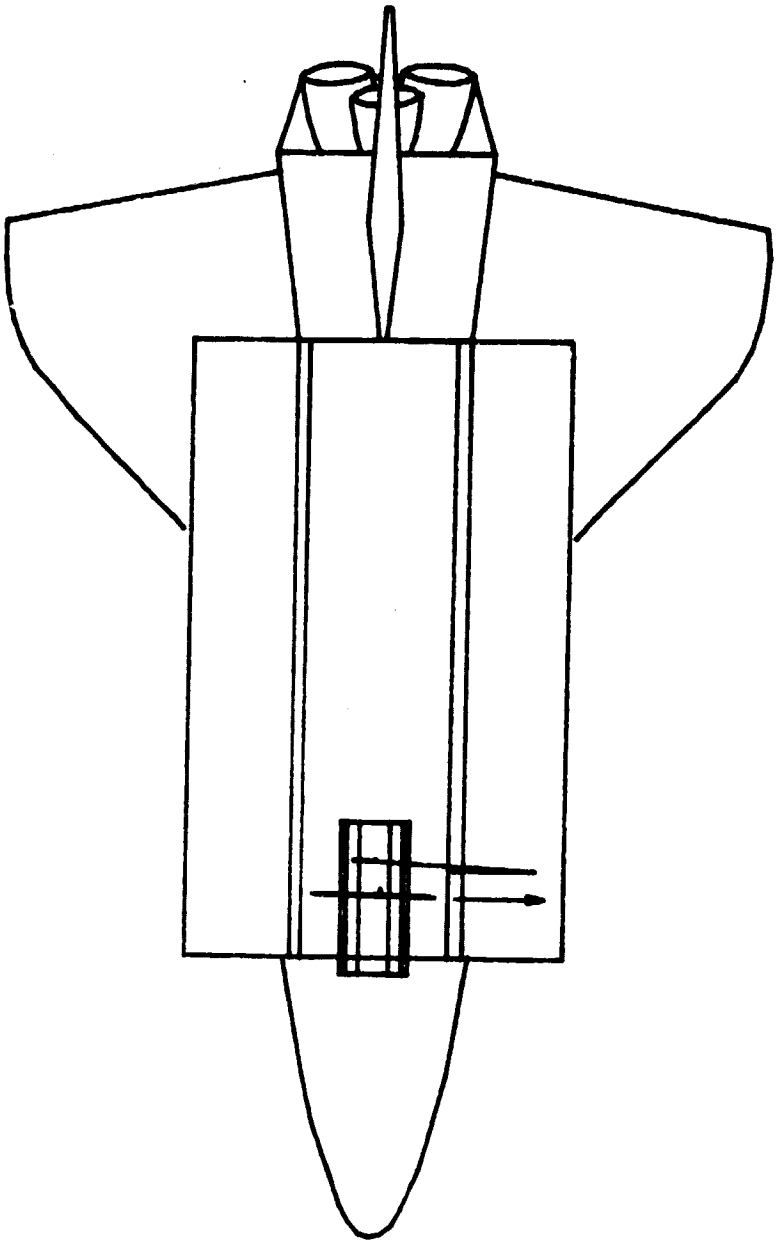

Fig. 21e

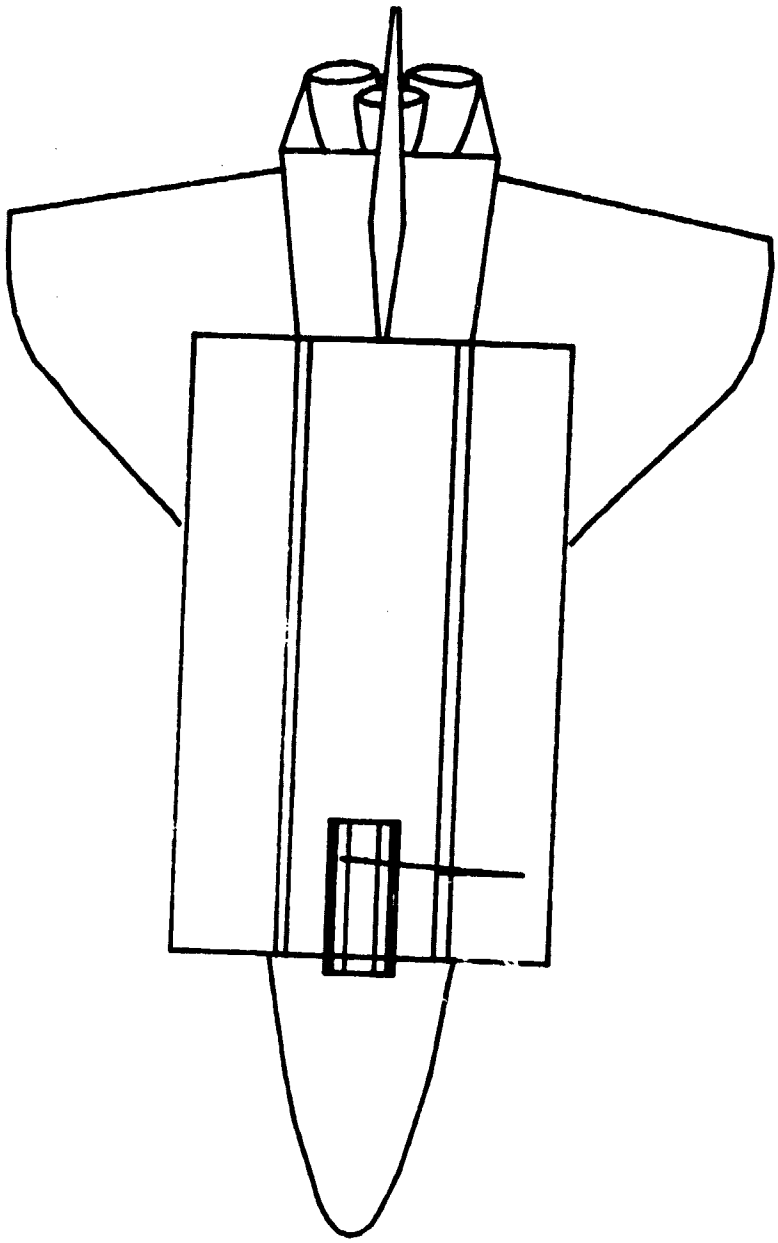

Fig. 21f

4.0 PDRSS ANALYSIS

Eight jettison simulations were made with the PDRSS. A separate simulation was made for the +Y panel jettison and the -Y panel jettison. Each of these cases was analyzed with the RMS in the position hold mode and then in the brakes on mode. Each of these cases was analyzed in the primary jettison configuration and then in the alternate jettison configuration.

For jettison of the -Y panel in the primary configuration, the wrist yaw joint is near a singularity. In this case, the PDRSS flexibility model becomes unstable. In order to execute a successful PDRSS analysis for this case, it was necessary to assume a rigid boom model of the RMS. However, the gearbox flexibility was still included.

It was observed that some of the loads on this simulation were appreciably higher than on any of the other simulations. In order to determine if this increase was mostly due to the rigid boom model or to the singularity, another simulation of the +Y panel jettison, in the primary configuration in the position hold mode was made, but with rigid RMS booms assumed. This particular configuration is not near a singularity. The results were compared with those for the same configuration, but with flexible booms assumed. Generally, there was no appreciable difference between the two. Therefore, it can be concluded that the bulk of the higher loads observed on the simulations with the rigid booms and the singularity are due to the singularity.

The PDRSS simulations were for a period of ten seconds after initiation of the jettison sequence. Recall that the panel is fully jettisoned after 1.54 seconds.

The forces and moments exerted on the RMS were determined for the end effector, the wrist yaw joint, the wrist pitch joint, the elbow pitch joint, the shoulder pitch joint, the Rockwell/Spar Interface, and the Manipulator Position Mechanism (MPM)/Longeron Interface. End effector excursions and rotations were also determined.

One important observation is that the results of the simulations in the position hold mode are exactly the same as those of otherwise similar simulations in the brakes on mode. This is because the loads about the joint drive axes do not exceed the motor static friction levels and thus, the joints do not move.

The RMS joint coordinate systems are described in Figure 22. The peak forces and moments, and end effector excursions and rotations are tabulated in Tables XII & XIII respectively.

Even the highest loads encountered in this study, those for the configuration near the wrist yaw singularity, do not exceed the drive torques generated by the joints themselves. The loads due to solar panel jettison for those configurations which are not near a singularity are typically much lower. Comparing the peak loads to the operational loads specified in References 6 & 7 and recognizing that these loads will only occur twice during the mission, it can be seen that the arm and the longeron can easily tolerate these loads.

End effector excursions and rotations due to solar panel jettison are negligibly small.

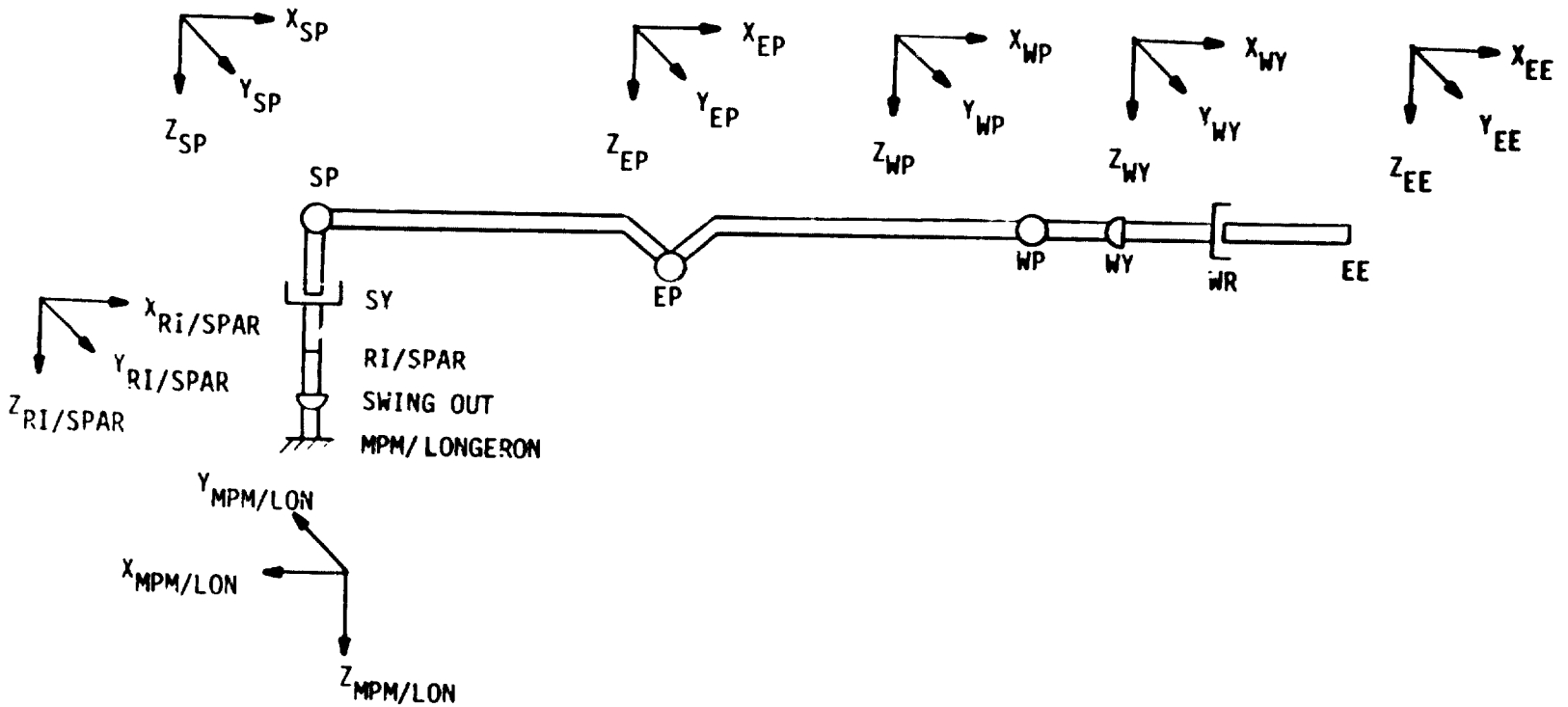

FIG. 22

RMS JOINT COORDINATE SYSTEMS

TABLE XII

MAXIMUM LOADS ON RMS

F = Force (lbs)	Primary Configuration		Alternate Configuration	
M = Moment (ft-lbf)	Position Hold/Brakes On		Position Hold/Brakes On	
	Panel Jettisoned		Panel Jettisoned	
	+Y	-Y	+Y	-Y
	F_X .89	4.97	1.02	1.27
	F_Y 1.36	1.61	1.06	.97
End Effector	F_Z 2.25	1.10	1.23	1.15
w.r.t. Wrist Yaw System	M_X 13.60	9.89	10.09	10.10
	M_Y 50.11	145.85	17.93	17.18
	M_Z 16.40	10.32	15.03	14.76
	F_X .89	4.97	1.02	1.27
	F_Y 1.36	1.61	1.06	.97
Wrist Yaw	F_Z 2.25	1.10	1.23	1.15
w.r.t. Wrist Yaw System	M_X 13.60	9.89	10.09	10.10
	M_Y 44.26	143.63	12.30	11.78
	M_Z 16.48	10.16	10.50	10.18
	F_X .90	1.98	1.00	1.27
	F_Y 1.17	4.88	1.05	.97
st Pitch	F_Z 2.25	1.10	1.23	1.15
.t. Wrist Pitch System	M_X 44.41	143.59	10.32	10.06
	M_Y 14.97	8.27	11.28	10.47
	M_Z 16.38	10.27	9.46	10.26
	F_X 2.23	1.86	.88	1.21
	F_Y 1.17	4.88	1.05	.97
Elbow Pitch	F_Z .95	1.37	1.34	.88
w.r.t. Elbow Pitch System	M_X 36.60	139.70	12.71	13.66
	M_Y 13.99	24.56	21.78	11.99
	M_Z 32.85	70.89	17.41	15.17
	F_X 2.19	1.74	1.33	1.15
	F_Y 1.17	4.88	1.05	.97
Shoulder Pitch	F_Z 1.01	1.02	.88	1.12
w.r.t.Shoulder Pitch System	M_X 14.07	37.86	16.47	12.01
	M_Y 19.60	35.97	32.71	26.22
	M_Z 52.45	253.50	31.43	35.44
	F_X 1.01	4.77	1.07	1.00
	F_Y 1.51	1.96	.96	1.14
Rockwell/Spar Interface	F_Z 2.10	1.58	1.28	1.19
w.r.t. Longeron System	M_X 34.87	95.04	34.81	28.41
	M_Y 49.13	251.55	37.49	38.09
	M_Z 14.52	10.23	10.41	10.38

TABLE XII (Continued)

		Panel Jettisoned		Panel Jettisoned	
		+Y	-Y	+Y	-Y
Manipulator Position Mechanism/Longeron Interface w.r.t. Orbiter Body Axis System	F_X	1.01	4.77	1.07	1.00
	F_Y	.72	1.88	1.11	1.15
	F_Z	2.48	1.53	1.17	1.42
	M_X	35.45	96.87	35.60	29.72
	M_Y	49.16	244.81	39.64	40.36
	M_Z	21.99	78.46	10.78	12.79

TABLE XIII

MAXIMUM END EFFECTOR EXCURSIONS AND ROTATIONS

F = Force (lbs)		Primary Configuration		Alternate Configuration	
M = Moment (ft-lbf)		Position Hold/Brakes On		Position Hold/Brakes On	
		Panel Jettisoned		Panel Jettisoned	
		+Y	-Y	+Y	-Y
Maximum End Effector Excursion w.r.t. Orbiter Body Axis System (inches)	X	.043	.036	.008	.007
	Y	.168	.156	.192	.132
	Z	.041	.060	.072	.040
		Panel Jettisoned		Panel Jettisoned	
		+Y	-Y	+Y	-Y
Maximum End Effector Rotation w.r.t. Orbiter Rotation Axis system (degrees)	Yaw	.024	.003	.033	.018
	Pitch	.004	.002	.002	.001
	Roll	.022	No Data	.002	No Data

5.0 CONCLUSIONS AND RECOMMENDATIONS

Based on the findings of this study, the following conclusions and recommendations are made:

(1) The loads on the RMS resulting from the jettisoning of the solar panels are well within the limits of the RMS for the configurations analyzed in this study, even though one of those configurations is near a wrist yaw singularity.

(2) The motion of the payload due to solar panel jettison is negligible.

(3) There is no difference in loads and end effector excursions between otherwise similar configurations analyzed in the position hold mode or in the brakes on mode. This is because the loads about the joint drive axes never exceed the motor static friction level and thus, the joints do not move.

The decisions to use the primary or alternate jettison configuration and to use the position hold mode or the brakes on mode should be based on considerations other than RMS structural loads due to solar panel jettison.

6.0 REFERENCES

1. "SMM Solar Panel Jettison and Recontact Analysis" MDTSCO-HAD, 28 September 1979, Design Note No. 1.4-DV-D1145-001.

2. "Updated Analysis of Solar Array System Jettison, Solar Max Mission", Hughes Aircraft Co., 2 November 1978, Ref. 4091.2/732.

3. "SMM Mass Properties Report. Mega Engineering, Silver Spring, Md., 4 September 1979, Contract No. NAS5-23430, Mod. 31.

4. SMM Scale Drawings, Goddard Space Flight Center, June 1979, Drawing SK5657, Sheets 1 & 2.

5. "Desired Orbiter Attitude for SMM Panel Jettison", MDTSCO-HAD, Memo E916-638, October 17, 1979.

6. "Load Specification SRMS Manipulator Arm", SPAR-SG.409,ISSUE E.

7. "Analysis of PDRS Data", Enclosure 15 of Minutes of 13th Meeting of the PDRS Working Group, JSC, Jan 23-25, 1979.

GOVERNMENT PRINTING OFFICE 1980—671-099/15